

# Efimov States in Nuclear and Particle Physics

HANS-WERNER HAMMER\*

*Helmholtz-Institut für Strahlen- und Kernphysik (Theorie) and Bethe Center*

*for Theoretical Physics, Universität Bonn, 53115 Bonn, Germany*

*Email: hammer@hiskp.uni-bonn.de*

LUCAS PLATTER

*Institute for Nuclear Theory, University of Washington, Seattle, WA 98195,*

*USA*

*Department of Physics, The Ohio State University, Columbus, OH 43210, USA*

*Email: lplatter@phys.washington.edu*

**Key Words** Universality, Efimov physics, few-body systems, discrete scale invariance, hyperspherical formalism, effective field theory

**Abstract** Particles with resonant short-range interactions have universal properties that do not depend on the details of their structure or their interactions at short distances. In the three-body system, these properties include the existence of a geometric spectrum of three-body Efimov states and a discrete scaling symmetry leading to log-periodic dependence of observables on the scattering length. Similar universal properties appear in the four-body system and possibly higher-body systems as well. For example, universal four-body states have recently been predicted and observed in experiment. These phenomena are often referred to as “Efimov Physics”. We review their theoretical description and discuss applications in different areas of physics with a special emphasis on nuclear and particle physics.

## CONTENTS

Introduction . . . . .	3
Physics of the Efimov Effect . . . . .	5
<i>History</i> . . . . .	5
<i>Hyperspherical Methods</i> . . . . .	7
<i>Efimov Spectrum</i> . . . . .	11
<i>Universal Properties</i> . . . . .	13
<i>Observation in Ultracold Atoms</i> . . . . .	15
Applications in Nuclear Physics . . . . .	18
<i>Few-Nucleon System</i> . . . . .	18
<i>Quark Mass Dependence and Infrared Limit Cycle</i> . . . . .	25
<i>Halo Nuclei</i> . . . . .	29
<i>Three-Alpha System and Coulomb Interaction</i> . . . . .	33
Applications in Particle Physics . . . . .	34
<i>Hadronic Molecules</i> . . . . .	34
Summary and Outlook . . . . .	36

## 1 Introduction

The scattering of particles with sufficiently low kinetic energy is determined by their S-wave scattering length  $a$ . This is the case if their de Broglie wavelengths are large compared to the range of the interaction.

Generically, the scattering length  $a$  is comparable in magnitude to the range  $\ell$  of the interaction:  $|a| \sim \ell$ . In exceptional cases, the scattering length can be much larger in magnitude than the range:  $|a| \gg \ell$ . Such a large scattering length requires the fine-tuning of a parameter characterizing the interactions to the neighborhood of a critical value at which  $a$  diverges to  $\pm\infty$ . If the scattering length is large, the particles exhibit properties that depend on  $a$  but are insensitive to the range and other details of the short-range interaction. These properties are universal in the sense that they apply equally well to any nonrelativistic particle with short range interactions that produce a large scattering length [1, 2].

For example, in the case of equal-mass particles with mass  $m$  and  $a > 0$ , there is a two-body bound state near the scattering threshold with binding energy  $B_d = \hbar^2/(ma^2)$ . The corrections to this formula are suppressed by powers of  $\ell/a$ . This bound state corresponds to a pole of the two-particle scattering amplitude at  $E = -B_d$ . If the scattering length is negative, there is a universal virtual state which corresponds to a pole on the unphysical second sheet in the complex energy plane.

The key evidence for universal behavior in the three-body system was the discovery of the Efimov effect in 1970 [3]. In the unitary limit  $1/a \rightarrow 0$ , the two-body bound state is exactly at the two-body scattering threshold  $E = 0$ . Efimov showed that in this limit there are infinitely many, arbitrarily-shallow three-body bound states whose binding energies  $B_t^{(n)}$  have an accumulation point at  $E = 0$ . The Efimov effect is just one aspect of universal properties in the three-body system. It has universal properties not only in the unitary limit, but whenever the scattering length is large compared to the range  $\ell$ . In particular, the log-periodic scattering length dependence of observables is a unique consequence of Efimov physics.

Although well established theoretically, the unambiguous identification of Efimov states in nature is difficult since typical systems are neither in the unitary limit nor can the scattering length be varied. The probably simplest example in nuclear physics is the triton. The triton can be interpreted as the ground state of an Efimov spectrum in the  $pnn$ -system with total spin  $J = 1/2$ . Since the ratio

$\ell/a$  is only about one third, the whole spectrum contains only one state but the low-energy properties of the triton can be described in this scenario. A promising system for observing several Efimov states is  $^4\text{He}$  atoms, which have a scattering length that is more than a factor of 10 larger than the range of the interaction. Calculations using accurate potential models indicate that the system of three  $^4\text{He}$  atoms has two three-body bound states or trimers. The ground-state trimer can be interpreted as an Efimov state, and it has been observed in experiments involving the scattering of cold jets of  $^4\text{He}$  atoms from a diffraction grating [4]. The excited trimer is universally believed to be an Efimov state, but it has not yet been observed.

The rapid development of the field of cold atom physics has opened up new opportunities for the experimental study of Efimov physics. This is made possible by two separate technological developments. One is the technology for cooling atoms to the extremely low temperatures where Efimov physics plays a crucial role. The other is the technology for controlling the interactions between atoms. By tuning the magnetic field to a Feshbach resonance, the scattering lengths of the atoms can be controlled experimentally and made arbitrarily large. Both developments were crucial in recent experiments that provided the first indirect evidence for the existence of Efimov states in ultracold atoms [5].

Overviews of Efimov physics in ultracold atomic gases can be found in Refs. [1, 2, 6]. In this review, we focus on universal aspects and Efimov states in nuclear and particle physics. Even though the scattering length can not be varied, there are many systems close to the unitary limit where Efimov physics is relevant. They include few-nucleon systems, halo nuclei, and weakly bound hadronic molecules. These systems can be described in a universal effective field theory (EFT) that implements an expansion around the unitary limit. Three-body bound states can be interpreted as Efimov trimers.

In the next section we will review the physics of the Efimov effect starting with a brief account of the history. In the following sections, we will discuss applications in nuclear and particle physics. We will end with a summary and outlook.

## 2 Physics of the Efimov Effect

### 2.1 History

The first hints on universal behavior in the three-body system came from the discovery of the Thomas collapse in 1935 [7] which is closely related to the Efimov effect. Thomas studied the zero-range limit for potentials with a single two-body bound state with fixed energy. Using a variational argument, he showed that the binding energy  $B_t^{(0)}$  of the deepest three-body bound state diverges to infinity in this limit. Thus the spectrum of three-body bound states is unbounded from below.

Further progress occurred by applying the zero-range limit to the three-nucleon system. An integral equation for S-wave neutron-deuteron scattering using zero-range interactions was derived by Skorniakov and Ter-Martirosian in 1957 [8]. For the spin-quartet channel, this integral equation has no bound state solutions and is well behaved. In the spin-doublet channel, however, it has solutions for arbitrary energy [9], including bound state solutions. If the solution is fixed by requiring some three-body energy, the resulting equation still has a discrete spectrum that extends to minus infinity in agreement with the earlier result of Thomas [10, 11]. Although a prediction for the spin-doublet neutron-deuteron scattering length was obtained using the triton binding energy as input [12], most work afterwards focused on finite range forces which avoid this pathology at high energies.

In 1970, Efimov realized that one should focus on the physics at low energies,  $E \ll \hbar^2/(m\ell^2)$ , and not on the deepest states. In this limit, where zero-range forces are adequate, he found some surprising results [3]. He pointed out that when  $|a|$  is sufficiently large compared to the range  $\ell$  of the potential, there is a sequence of three-body bound states whose binding energies are spaced roughly geometrically in the interval between  $\hbar^2/(m\ell^2)$  and  $\hbar^2/(ma^2)$ . As  $|a|$  is increased, new bound states appear in the spectrum at critical values of  $a$  that differ by multiplicative factors of  $e^{\pi/s_0}$ , where  $s_0$  depends on the statistics and the mass ratios of the particles. In the case of spin-doublet neutron-deuteron scattering and for three identical bosons,  $s_0$  is the solution to the transcendental equation

$$s_0 \cosh \frac{\pi s_0}{2} = \frac{8}{\sqrt{3}} \sinh \frac{\pi s_0}{6}. \quad (1)$$

Its numerical value is  $s_0 \approx 1.00624$ , so  $e^{\pi/s_0} \approx 22.7$ . As  $|a|/\ell \rightarrow \infty$ , the asymp-

otic number of three-body bound states is

$$N \longrightarrow \frac{s_0}{\pi} \ln \frac{|a|}{\ell}. \quad (2)$$

In the limit  $a \rightarrow \pm\infty$ , there are infinitely many three-body bound states with an accumulation point at the three-body scattering threshold with a geometric spectrum:

$$B_t^{(n)} = (e^{-2\pi/s_0})^{n-n_*} \hbar^2 \kappa_*^2 / m, \quad (3)$$

where  $m$  is the mass of the particles and  $\kappa_*$  is the binding wavenumber of the branch of Efimov states labeled by  $n_*$ . The geometric spectrum in (3) is the signature of a discrete scaling symmetry with scaling factor  $e^{\pi/s_0} \approx 22.7$ . It is independent of the mass or structure of the identical particles and independent of the form of their short-range interactions. The Efimov effect can also occur in other three-body systems if at least two of the three pairs have a large S-wave scattering length but the numerical value of the asymptotic ratio may differ from the value 22.7.

A formal proof of the Efimov effect was subsequently given by Amado and Noble [13, 14]. The Thomas and Efimov effects are closely related. The deepest three-body bound states found by Thomas's variational calculation can be identified with the deepest Efimov states [15]. The mathematical connection of the Efimov effect to a limit cycle was discussed in [16].

The universal properties in the three-body system with large scattering length are not restricted to the Efimov effect. The dependence of three-body observables on the scattering length or the energy is characterized by scaling behavior modulo coefficients that are log-periodic functions of  $a$  [17, 18]. This behavior is characteristic of a system with a discrete scaling symmetry. We will refer to universal aspects associated with a discrete scaling symmetry as Efimov physics.

In 1981, Efimov proposed a new approach to the low-energy few-nucleon problem in nuclear physics that, in modern language, was based on perturbation theory around the unitary limit [19]. Remarkably, this program works reasonably well in the three-nucleon system at momenta small compared to  $M_\pi$ . The Efimov effect makes it necessary to impose a boundary condition on the wave function at short distances. The boundary condition can be fixed by using either the spin-doublet neutron-deuteron scattering length or the triton binding energy as input. If the deuteron binding energy and the spin-singlet nucleon-nucleon scattering length are used as the two-body input and if the boundary condition

is fixed by using the spin-doublet neutron-deuteron scattering length as input, the triton binding energy is predicted with an accuracy of 6%. The accuracy of the predictions can be further improved by taking into account the effective range as a first-order perturbation [20]. Thus the triton can be identified as an Efimov state associated with the deuteron and the spin-singlet virtual state being a  $pn$  state with large scattering length [19].

In the three-nucleon system, this program was implemented within an effective field theory framework by Bedaque, Hammer, and van Kolck [21–23]. In Ref. [23], they found that the renormalization of the effective field theory requires a  $SU(4)$ -symmetric three-body interaction with an ultraviolet limit cycle. The three-body force depends on a parameter  $\Lambda_*$  that is determined through a renormalization condition that plays the same role as Efimov’s boundary condition.  $SU(4)$ -symmetry was introduced by Wigner in 1937 as generalization of the  $SU(2) \times SU(2)$  spin-isospin symmetry, allowing for a mixing of spin and isospin degrees of freedom in symmetry transformations [24]. It is satisfied to a high degree in the energy spectra of atomic nuclei. Exact Wigner symmetry requires the S-wave scattering lengths in the spin-triplet and spin-singlet channels to be equal. However, if the two-body scattering lengths are large, it is a very good approximation even if they are different since the symmetry-breaking terms are proportional to the inverse scattering lengths [25].

This effective field theory (EFT) is ideally suited to calculating corrections to the universal results in the scaling limit. Its application to few-nucleon physics will be discussed in Section 3.

## 2.2 Hyperspherical Methods

Coordinate space methods have proven to be a valuable tool for the analysis of the three-body problem with short-range interactions [17, 26, 27]. In this subsection we will introduce the hyperspherical approach that has been used to obtain important results about the Efimov spectrum. The material of this subsection is based on the discussion of the hyperradial formalism in the review of Ref. [1]. For three particles of equal mass the Jacobi coordinates are defined as:

$$\mathbf{r}_{ij} = \mathbf{r}_i - \mathbf{r}_j ; \quad \mathbf{r}_{k,ij} = \mathbf{r}_k - \frac{1}{2}(\mathbf{r}_i + \mathbf{r}_j) , \quad (4)$$

where the triple  $(ijk)$  is a cyclic permutation of the particle indices (123). The hyperradius  $R$  and hyperangle  $\alpha_k$  are then defined by

$$R^2 = \frac{1}{3}(\mathbf{r}_{12}^2 + \mathbf{r}_{23}^2 + \mathbf{r}_{31}^2) = \frac{1}{2}\mathbf{r}_{ij}^2 + \frac{2}{3}\mathbf{r}_{k,ij}^2; \quad \alpha_k = \arctan\left(\frac{\sqrt{3}|\mathbf{r}_{ij}|}{2|\mathbf{r}_{k,ij}|}\right). \quad (5)$$

In the center-of-mass system the Schrödinger equation in hyperspherical coordinates is given by

$$\left(T_R + T_{\alpha_k} + \frac{\Lambda_{k,ij}^2}{2mR^2} + V(R, \Omega)\right) \Psi(R, \alpha, \Omega) = E\Psi(R, \alpha, \Omega), \quad (6)$$

with

$$T_R = \frac{\hbar^2}{2m}R^{-5/2}\left(-\frac{\partial}{\partial R^2} + \frac{15}{4R^2}\right)R^{5/2}, \quad (7)$$

$$T_{\alpha} = \frac{\hbar^2}{2mR^2}\frac{1}{\sin 2\alpha}\left(-\frac{\partial^2}{\partial \alpha^2} - 4\right)\sin 2\alpha, \quad (8)$$

$$\Lambda_{k,ij}^2 = \frac{\mathbf{L}_{ij}^2}{\sin^2 \alpha_k} + \frac{\mathbf{L}_{k,ij}^2}{\cos^2 \alpha_k}, \quad (9)$$

where  $\Omega = (\theta_{ij}, \phi_{ij}, \theta_{k,ij}, \phi_{k,ij})$  and the  $L$ s that appear in Eq. (9) are the usual angular-momentum operators with respect to these angles.

We will assume that the potential  $V$  depends only on the magnitude of the inter-particle separation and write

$$V(\mathbf{r}_1, \mathbf{r}_2, \mathbf{r}_3) = V(r_{12}) + V(r_{23}) + V(r_{31}). \quad (10)$$

We now employ the usual Faddeev decomposition of  $\psi$  for three identical bosons and neglect subsystem angular momentum

$$\Psi(R, \alpha, \Omega) = \psi(R, \alpha_1) + \psi(R, \alpha_2) + \psi(R, \alpha_3). \quad (11)$$

The solution of the corresponding Faddeev equation can then be expanded in a set of eigenfunctions of the hyperangular operator, i.e.

$$\psi(R, \alpha) = \frac{1}{R^{5/2}\sin(2\alpha)} \sum_n f_n(R) \phi_n(R, \alpha). \quad (12)$$

This leads to separate differential equations for the hyperangular functions  $\phi_n$  and the hyperradial functions  $f_n$ . We obtain in particular for the hyperradial functions

$$\begin{aligned} Ef_n(R) = & \left[ \frac{\hbar^2}{2m} \left( -\frac{\partial^2}{\partial R^2} + \frac{15}{4R^2} \right) + V_n(R) \right] f_n(R) \\ & + \sum_m \left[ 2P_{nm}(R) \frac{\partial}{\partial R} + Q_{nm}(R) \right] f_m(R), \end{aligned} \quad (13)$$



with the hyperradial potential  $V_n(R)$  defined by

$$V_n(R) = (\lambda_n(R) - 4) \frac{\hbar^2}{2mR^2}, \quad (14)$$

and  $P_{nm}(R)$  and  $Q_{nm}(R)$  potentials that induce coupling between different hyperradial channels [1].

For hyperradii  $R$  which are much larger than the range  $\ell$  over which  $V$  is non-zero, the solution of the equation for the hyperangular function  $\phi_n$  for large  $\alpha$  is

$$\phi_n^{(\text{high})}(\alpha) \approx \sin \left[ \sqrt{\lambda_n} \left( \frac{\pi}{2} - \alpha \right) \right]. \quad (15)$$

On the other hand, for  $R \gg \ell$  and small  $\alpha$ , it can be shown that the solution for the hyperangular part can be written as

$$\phi_n^{(\text{low})}(\alpha) = A \psi_0(\sqrt{2}R\alpha) - \frac{8\alpha}{\sqrt{3}} \sin \left( \sqrt{\lambda_n} \frac{\pi}{6} \right), \quad (16)$$

where  $A$  is a constant and  $\psi_0$  is the zero-energy solution to a two-body Schroedinger equation with the two-body potential  $V$

$$\psi_k(r) = \frac{\sin(kr + \delta(k))}{k} = \frac{\sin \delta(k)}{k} [\cos(kr) + \cot \delta \sin(kr)]. \quad (17)$$

As  $k \rightarrow 0$  this yields  $\psi_0(r) = r - a$ , and we can use this asymptotic two-body wave function in Eq. (16). This gives

$$\phi_n^{(\text{low})}(\alpha) = A(\sqrt{2}R\alpha - a) - \frac{8\alpha}{\sqrt{3}} \sin \left( \sqrt{\lambda_n} \frac{\pi}{6} \right). \quad (18)$$

But, since  $V = 0$  in this region, this result must be consistent with Eq. (15). This is achieved by the choice

$$A = -\frac{1}{a} \sin \left[ \sqrt{\lambda_n} \frac{\pi}{2} \right], \quad (19)$$

which ensures that  $\phi_n(\alpha)$  is continuous across the boundary between “low” and “high” solutions at  $\alpha \approx \ell/R$ , and the condition

$$\cos \left( \sqrt{\lambda_n} \frac{\pi}{2} \right) - \frac{8}{\sqrt{3\lambda_n}} \sin \left( \sqrt{\lambda_n} \frac{\pi}{6} \right) = \sqrt{\frac{2}{\lambda_n}} \sin \left( \sqrt{\lambda_n} \frac{\pi}{2} \right) \frac{R}{a}, \quad (20)$$

on  $\lambda_n$ , which ensures that  $\phi_n(\alpha)$  has a continuous first derivative as  $\alpha \rightarrow \ell/R$ . We note that if these equations are satisfied  $\lambda_n$ , and hence  $\phi_n$ , is independent of  $R$  for  $R \ll |a|$ . Indeed, as long as Eqs. (20) and (19) are satisfied the form (15) is the result for  $\phi$  for all  $\alpha$  such that  $\alpha > \ell/R$ . Solving Eq. (20) in the limit  $R \ll |a|$  we find the lowest eigenvalue

$$\lambda_0 = -s_0^2 \left( 1 + 1.897 \frac{R}{a} \right), \quad (21)$$

with  $s_0 = 1.00624\dots$ . This is the only negative eigenvalue, and hence only this channel potential is attractive. So, if we now focus on the unitary limit, where  $|a| \rightarrow \infty$ , we have  $\lambda_0 = -s_0^2$ . Since it can also be shown that the coupling potentials  $P_{nm}$  and  $Q_{nm}$  vanish in this regime, the hyperradial equation (13) in the lowest channel becomes

$$\frac{\hbar^2}{2m} \left( -\frac{\partial^2}{\partial R^2} - \frac{s_0^2 + \frac{1}{4}}{R^2} \right) f_0(R) = E f_0(R). \quad (22)$$

This equation will hold for  $R \gg \ell$ . If we desire a solution for negative  $E$  the requirement of normalizability for  $f_0$  mandates that

$$f_0^{(0)}(R) = \sqrt{R} K_{is_0}(\sqrt{2}\kappa R), \quad (23)$$

where the superscript (0) indicates that we are working in the unitary limit, while the subscript 0 refers to the solution for the hyperchannel corresponding to  $\lambda_0$ , which is the only one that supports bound states. The binding energy of these bound states is related to the  $\kappa$  of Eq. (23) by

$$B_t \equiv \frac{\hbar^2 \kappa^2}{m}. \quad (24)$$

Since the attractive  $1/R^2$  potential produces a spectrum that is unbounded from below some other short-distance physics is needed in order to stabilize the system. If the two-body potential is known this short-distance physics is provided by the two-body potential  $V$ , that becomes operative for  $R \sim \ell$ . But an alternative approach is to add an additional term to Eq. (22) that summarizes the impact of the two-body  $V$ . Here we take this potential to be a surface delta function at a radius  $1/\Lambda$  [28]

$$V_{SR}(R) = H_0(\Lambda) \Lambda^2 \delta \left( R - \frac{1}{\Lambda} \right), \quad (25)$$

with  $H_0$  adjusted as a function of  $\Lambda$  such that the binding energy of a particular state, say  $B_t^{(n_*)}$  (with a corresponding  $\kappa_*$ , given by (24)), is reproduced. Note that since  $V_{SR}$  is operative only at small hyperradii  $R \sim 1/\Lambda$  it corresponds to a three-body force. (See Ref. [29] for a realization of this in a momentum-space formalism.) In physical terms we anticipate  $\ell \sim 1/\Lambda$ , since we know that once we consider hyperradii of order  $1/\Lambda$  the potential  $V$  starts to affect the solutions.

Given that our focus is on predictions of the theory that are independent of details of  $V$  we can consider the extreme case and take the limit  $\ell \rightarrow 0$ . In this limit the form of  $K_{is_0}$  as  $R \rightarrow 0$  guarantees that once  $H_0$  is fixed to give a bound state at  $B_t^{(n_*)}$ , the other binding energies in this hyperradial eigenchannel form

a geometric spectrum. Namely,  $B_t^{(n)} = \hbar^2 \kappa_n^2 / m$  with

$$\kappa_n = \left( e^{-\pi/s_0} \right)^{n-n_*} \kappa_*, \quad (26)$$

with  $n_*$  the index of the bound state corresponding to  $\kappa_*$ . Eq. (26) will hold for all  $\kappa_n$  such that  $\kappa_n \ll \Lambda$ . (Note that now the subscript on  $\kappa$  denotes the index of the bound state in adiabatic channel zero.) The continuous scale invariance of the  $1/R^2$  potential has been broken down to a discrete scale invariance by the imposition of particular short-distance physics on the problem through the short-distance potential (25) [28].

It was subsequently shown that the discrete scale invariance of the three-body wavefunction which is exact in the limit of infinite scattering length and zero range also has implications for finite range. A perturbative calculation of the effect of a finite effective range on the bound state spectrum showed that the spectrum remains unchanged [30] and corrections to binding energies are of order  $(r_0/a)^2$  where  $r_0$  is the effective range of the interaction.

### 2.3 Efimov Spectrum

The hyperspherical methods discussed above can also be used to obtain the binding energy spectrum at finite scattering length. The short-distance boundary condition that was used to fix the binding energy in the unitary limit also determines the bound state spectrum at finite scattering length. The binding momentum  $\kappa_*$  introduced above can therefore be considered as a convenient parameter that determines the value of all universal few-body observable of the corresponding universality class.

The exact discrete scaling symmetry observed in the limit of infinite scattering length also exists if  $\kappa_*$  is kept fixed and  $a$  and other variables such as the energy are rescaled

$$\kappa_* \rightarrow \kappa_* , \quad a \rightarrow \mathcal{S}_0^m a , \quad E \rightarrow \mathcal{S}_0^{-2m} E . \quad (27)$$

Observables such as binding energy and cross sections scale with integer powers of  $\mathcal{S}_0 = \exp(\pi/s_0)$  under this symmetry. For example, the binding energy of an Efimov trimer which is a function of  $a$  and  $\kappa_*$  scales

$$B_t^{(n)}(\mathcal{S}_0^m a, \kappa_*) = \mathcal{S}_0^{-2m} B_t^{(n-m)}(a, \kappa_*) . \quad (28)$$

This implies for positive scattering length

$$B_t^{(n)}(a, \kappa_*) = F_n(2s_0 \ln(a\kappa_*)) \frac{\hbar^2 \kappa_*^2}{m} . \quad (29)$$

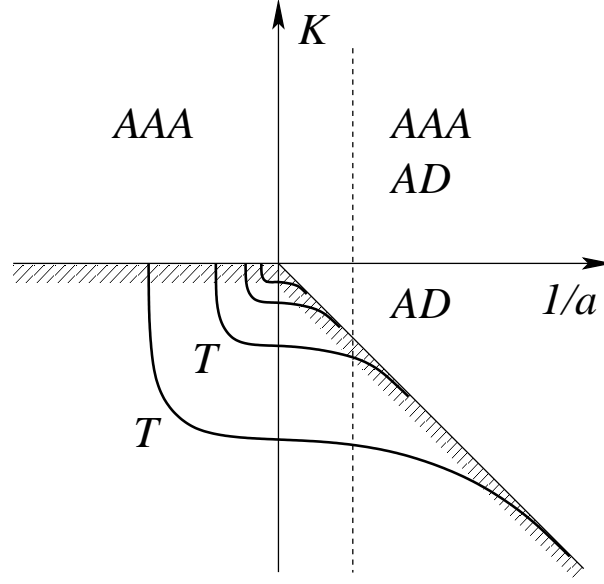


Figure 1: The Efimov plot for the three-body problem. We show  $K \equiv \text{sgn}(E)(m|E|)^{1/2}/\hbar$  versus the inverse scattering length. The allowed regions for three-atom scattering states and atom-dimer scattering states are labeled  $AAA$  and  $AD$ , respectively. The heavy lines labeled  $T$  are two of the infinitely many branches of Efimov states. The cross-hatching indicates the threshold for scattering states. States along the vertical dashed line have a fixed scattering length.

The function  $F_n$  parametrizes the scattering length dependence of all Efimov trimers exactly in the limit of vanishing range. The function  $F_n$  satisfies

$$F_n(x + 2m\pi) = (e^{-2\pi/s_0})^m F_{n-m}(x) . \quad (30)$$

The scattering length dependence of the bound state spectrum is shown in Fig. 1. We plot the quantity  $K \equiv \text{sgn}(E)(m|E|)^{1/2}/\hbar$  against the inverse scattering length. For bound states  $K$  corresponds to the binding momentum. The lines denote Efimov trimers below the threshold. The threshold for scattering states is denoted by the hatched area. Only a few of the infinitely many Efimov branches are shown. A given physical system has a fixed scattering length value and is denoted by the vertical dashed line. Changing the parameter  $\kappa_*$  by a factor  $\mathcal{S}_0$  corresponds to multiplying each branch of trimers with this factor without changing their shapes. One important result is that three-bound states exist for positive and negative scattering length. This is remarkable for the latter case since the two-body subsystem is unbound for  $a < 0$ . At a negative scattering length that we denote with  $a'_*$ , a bound state with a give  $\kappa_*$  has zero binding energy. As the scattering length is increased the binding energy gets larger until it crosses the atom-dimer threshold at the positive scattering length  $a_*$ . The

quantities  $a_*$  and  $a'_*$  can also be used to quantify a universality class of Efimov states.

## 2.4 Universal Properties

Other calculable observables will also display the discrete scaling symmetry that we just discussed for the bound state spectrum. The atom-dimer cross section fulfils for example the constraint

$$\sigma_{\text{AD}}(\mathcal{S}_0^{-2m}E; \mathcal{S}_0^m a, \kappa_*) = \mathcal{S}_0^{2m} \sigma_{\text{AD}}(E; a, \kappa_*) \quad (31)$$

under rescaling. At  $E = 0$  the cross section is related to the atom-dimer scattering length  $\sigma_{\text{AD}} = 4\pi|a_{\text{AD}}|^2$ . This implies that the atom-dimer scattering length can be written as

$$a_{\text{AD}} = f(2s_0 \ln(a\kappa_*))a, \quad (32)$$

where  $f(x)$  is periodic function with period  $2\pi$ .

An observable that has been crucial for the experimental detection of Efimov physics in ultracold atoms is the three-body recombination rate. In ultracold gases, atoms can undergo inelastic three-body collisions in which a two-body bound state is formed. The dimer and remaining atom gain kinetic energy in this process and can leave the atomic trap. Such processes lead to a measurable loss of particles in the atomic trap. For negative scattering length, atoms can only recombine into deep dimers that have binding energy of order  $\hbar^2/(mR^2)$ . For positive scattering length, atoms can recombine into shallow dimers with binding energy  $\hbar^2/(ma^2)$  and deep dimers. The recombination rate that is a measure for the loss rate of atoms scales as  $\hbar a^4/m$  times a log-periodic coefficient that is a function of  $a$  and  $\kappa_*$ . The recombination rate constant  $\alpha$  can therefore be written as

$$\alpha(a) = g(2s_0 \ln(a\kappa_*)) \frac{\hbar a^4}{m}. \quad (33)$$

The analytic form of the function  $g(x)$  is known and can be found in [1, 6]. Here we want to focus on the qualitative features as shown in Fig. 2 for positive scattering length. At positive scattering length interference effects lead to log-periodically spaced minima in the recombination rate. At negative scattering length free atoms can only recombine into deep dimers. This process will be enhanced dramatically whenever an Efimov trimer is at threshold.

A different perspective on Efimov physics can be gained by keeping the two-body scattering length fixed and varying the three-body parameter. As a result

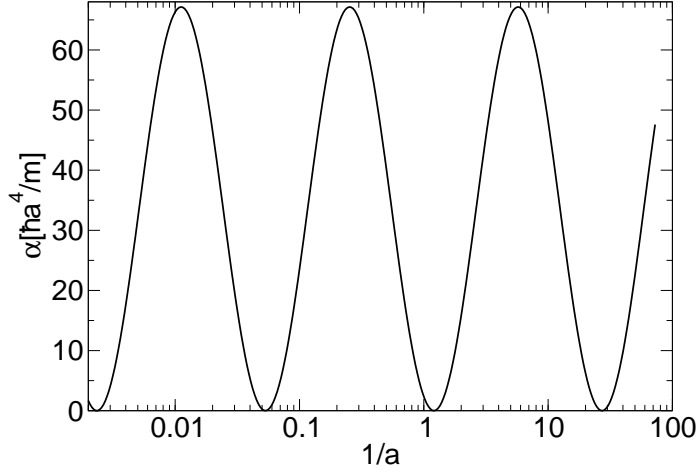


Figure 2: The recombination rate constant  $\alpha$  for positive scattering length  $a$  in units of  $\hbar a^4/m$  as a function of  $1/a$  (in arbitrary units).

all three-body observables are correlated and will lead to correlation lines when plotted against each other. One of them (well-known from nuclear physics) is the Phillips line [31], the correlation that results when the trimer binding energy is plotted against the atom-dimer scattering length. Such correlations had been observed frequently in nuclear physics, where different phase shift equivalent potentials were employed in few-body calculations.

Since one three-body parameter is required for a description of the three-body system with zero-range interactions it is natural to ask how many parameters are needed for calculations in the  $n$ -body system. A first step towards answering this question was performed in Ref. [32]. The authors of this work showed that the two-body scattering length and one three-body parameter are sufficient to make predictions for four-body observables. Results in a more detailed analysis [33] also lead to the conclusion that every trimer state is tied to two universal tetramer states with binding energies related to the binding energy of the next shallower trimer. In the unitary limit  $1/a = 0$ , the relation between the binding energies was found as:

$$B_4^{(0)} \approx 5 B_t \quad \text{and} \quad B_4^{(1)} \approx 1.01 B_t, \quad (34)$$

where  $B_4^{(0)}$  denotes the binding energy of the deeper of the two tetramer states and  $B_4^{(1)}$  the shallower of the two.

A recent calculation by von Stecher, d’Incao and Greene [34] supports these

findings and extends them to higher numerical accuracy. For the relation between universal three- and four-body bound states in the unitary limit, they found

$$B_4^{(0)} \approx 4.57 B_t \quad \text{and} \quad B_4^{(1)} \approx 1.01 B_t , \quad (35)$$

which is consistent with the results given in Eq. (34) within the numerical accuracy.

The results obtained by the Hammer and Platter in Ref. [33] were furthermore presented in the form of an extended Efimov plot, shown in Fig. 3. Four-body states must have a binding energy larger than the one of the deepest trimer state. The corresponding threshold is denoted by lower solid line in Fig. 3. The threshold for decay into the shallowest trimer state and an atom is indicated by the upper solid line. At positive scattering length, there are also scattering thresholds for scattering of two dimers and scattering of a dimer and two particles indicated by the dash-dotted and dashed lines, respectively. The vertical dotted line denotes infinite scattering length.

An extended version of this four-body Efimov plot was also presented by von Stecher, d’Incao and Greene in Ref. [34]. They calculated more states with higher numerical accuracy and extended the calculation of the four-body states to the thresholds where they become unstable. From these results they extracted the negative values of the scattering lengths at which the binding energies of the tetramer states become zero and found

$$a_{4,0}^* \approx 0.43a'_* \quad \text{and} \quad a_{4,1}^* \approx 0.92a'_* . \quad (36)$$

These numbers uniquely specify the relative position of three- and four-body recombination resonances. This was the key information for the subsequent observation of these states in ultracold atoms by Ferlaino et al. [35].

Calculations for larger number of particles using a model that incorporates the universal behavior of the three-body system were carried out by von Stecher [36]. His findings indicate that there is at least one  $N$ -body state tied to each Efimov trimer and numerical evidence was also found for a second excited 5-body state.

## 2.5 Observation in Ultracold Atoms

The first experimental evidence for Efimov physics in ultracold atoms was presented by Kraemer et al. [5] in 2006. This group used  $^{133}\text{Cs}$  atoms in the lowest hyperfine spin state. They observed resonant enhancement of the loss of atoms

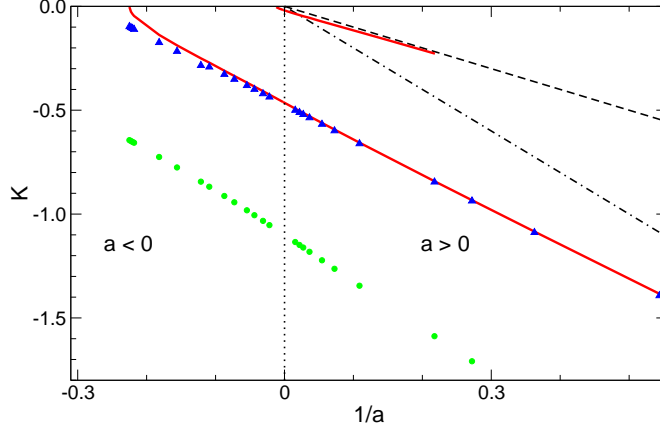


Figure 3: The extended Efimov plot for the four-body problem. We show  $K \equiv \text{sgn}(E)(m|E|)^{1/2}/\hbar$  versus the inverse scattering length. Both quantities are given in arbitrary units. The circles and triangles indicate the four-body ground and excited states, respectively, while the lower (upper) solid lines give the thresholds for decay into a ground state (excited state) trimer and a particle. The dash-dotted (dashed) lines give the thresholds for decay into two dimers (a dimer and two particles). The vertical dotted line indicates infinite scattering length.

from three-body recombination that can be attributed to an Efimov trimer crossing the three-atom threshold. Kraemer et al. also observed a minimum in the three-body recombination rate that can be interpreted as an interference effect associated with Efimov physics. In a subsequent experiment with a mixture of  $^{133}\text{Cs}$  atoms and dimers, Knoop et al. observed a resonant enhancement in the loss of atoms and dimers [37]. This loss feature can be explained by an Efimov trimer crossing the atom-dimer threshold [38]. The most exciting recent developments in the field of Efimov physics involve universal tetramer states. Ferlaino et al. observed two tetramers in an ultracold gas of  $^{133}\text{Cs}$  atoms [35] that confirm the results by Hammer and Platter [32, 33] and von Stecher, D’Incao and Greene [34].

Recent experiments with other bosonic atoms have provided even stronger evidence of Efimov physics in the three- and four-body sectors. Zaccanti et al. measured the three-body recombination rate and the atom-dimer loss rate in a ultracold gas of  $^{39}\text{K}$  atoms [39]. They observed two atom-dimer loss resonances and two minima in the three-body recombination rate at large positive values of the scattering length. The positions of the loss features are consistent with the universal predictions with discrete scaling factor 22.7. They also observed



loss features at large negative scattering lengths. Barontini et al. obtained the first evidence of the Efimov effect in a heteronuclear mixture of  $^{41}\text{K}$  and  $^{87}\text{Rb}$  atoms [40]. They observed 3-atom loss resonances at large negative scattering lengths in both the K-Rb-Rb and K-K-Rb channels, for which the discrete scaling factors are 131 and  $3.51 \times 10^5$ , respectively. Gross *et al.* measured the three-body recombination rate in an ultracold system of  $^7\text{Li}$  atoms [41]. They observed a 3-atom loss resonance at a large negative scattering length and a three-body recombination minimum at a large positive scattering length. The positions of the loss features, which are in the same universal region on different sides of a Feshbach resonance, are consistent with the universal predictions with discrete scaling factor 22.7. Pollack *et al.* measured the three-body recombination in a system of  $^7\text{Li}$  atoms in a hyperfine state different from the system considered by Gross *et al.* [42]. They observed a total of 11 three- and four-body loss features. The features obey the universal relations on each side of the Feshbach resonance separately, however, a systematic error of  $\sim 50\%$  is found when features on different sides of the Feshbach resonance are compared.

Efimov physics has also been observed in three-component systems of  $^6\text{Li}$  atom. For the three lowest hyperfine states of  $^6\text{Li}$  atoms, the three pair scattering lengths approach a common large negative value at large magnetic fields and all three have nearby Feshbach resonances at lower fields that can be used to vary the scattering lengths [43]. The first experimental studies of many-body systems of  $^6\text{Li}$  atoms in the three lowest hyperfine states have recently been carried out by Ottenstein et al. [44] and by Huckans et al. [45]. Their measurements of the three-body recombination rate revealed a narrow loss feature and a broad loss feature in a region of low magnetic field. Theoretical calculations of the three-body recombination rate supported the interpretation that the narrow loss feature arises from an Efimov trimer crossing the 3-atom threshold [46–48]. Very recently, another narrow loss feature was discovered in a much higher region of the magnetic field by Williams et al. [49] and by Jochim and coworkers. Williams et al. used measurements of the three-body recombination rate in this region to determine the complex three-body parameter that governs Efimov physics in this system. This parameter, together with the three scattering lengths as functions of the magnetic field, determine the universal predictions for  $^6\text{Li}$  atoms in this region of the magnetic field.

### 3 Applications in Nuclear Physics

The properties of hadrons and nuclei are determined by quantum chromodynamics (QCD), a non-abelian gauge theory formulated in terms of quark and gluon degrees of freedom. At low energies, however, the appropriate degrees of freedom are the hadrons. Efimov physics and the unitary limit can serve as a useful starting point for effective field theories (EFTs) describing hadrons and nuclei at very low energies. For convenience, we will now work in natural units where  $\hbar = c = 1$ .

In nuclear physics, there are a number of EFTs which are all useful for a certain range of systems [50–52]. At very low energies, where Efimov physics plays a role, all interactions can be considered short-range and even the pions can be integrated out. This so-called “pionless EFT” is formulated in an expansion of the low-momentum scale  $M_{low}$  over the high-momentum scale  $M_{high}$ . It can be understood as an expansion around the limit of infinite scattering length or equivalently around threshold bound states. Its breakdown scale is set by one-pion exchange,  $M_{high} \sim M_\pi$ , while  $M_{low} \sim 1/a \sim k$ . For momenta  $k$  of the order of the pion mass  $M_\pi$ , pion exchange becomes a long-range interaction and has to be treated explicitly. This leads to the chiral EFT whose breakdown scale  $M_{high}$  is set by the chiral symmetry breaking scale  $\Lambda_\chi$ . The pionless theory relies only on the large scattering length and is independent of the short-distance mechanism generating it. This theory is therefore ideally suited to unravel universal phenomena driven by the large scattering length such as limit cycle physics [53, 54] and the Efimov effect [3]. In this section, we will focus on the aspects of nuclear effective field theories related to Efimov physics. For more complete overviews of the application of effective field theories to nuclear phenomena in general, a number of excellent reviews are available [50–52, 55].

#### 3.1 Few-Nucleon System

In the two-nucleon system, the pionless theory reproduces the well known effective range expansion in the large scattering length limit. The renormalized S-wave scattering amplitude to next-to-leading order in a given channel takes the form

$$T_2(k) = \frac{4\pi}{m} \frac{1}{-1/a - ik} \left[ 1 - \frac{r_0 k^2/2}{-1/a - ik} + \dots \right], \quad (37)$$

where  $k$  is the relative momentum of the nucleons and the dots indicate corrections of order  $(M_{low}/M_{high})^2$  for typical momenta  $k \sim M_{low}$ . In the language

of the renormalization group, this corresponds to an expansion around the non-trivial fixed point for  $1/a = 0$  [56, 57]. The pionless EFT becomes very useful in the two-nucleon sector when external currents are considered and has been applied to a variety of electroweak processes. These calculations are reviewed in detail in Refs. [50, 51].

Here we focus on the three-nucleon system. It is convenient (but not mandatory) to write the theory using so-called “dimeron” auxiliary fields [58]. We need two dimeron fields, one for each S-wave channel: (i) a field  $t_i$  with spin (isospin) 1 (0) representing two nucleons interacting in the  $^3S_1$  channel (the deuteron) and (ii) a field  $s_a$  with spin (isospin) 0 (1) representing two nucleons interacting in the  $^1S_0$  channel [23]:

$$\begin{aligned} \mathcal{L} = & N^\dagger \left( i\partial_t + \frac{\vec{\nabla}^2}{2m} \right) N - t_i^\dagger \left( i\partial_t - \frac{\vec{\nabla}^2}{4m} - \Delta_t \right) t_i \\ & - s_a^\dagger \left( i\partial_t - \frac{\vec{\nabla}^2}{4m} - \Delta_s \right) s_a - \frac{g_t}{2} \left( t_i^\dagger N^T \tau_2 \sigma_i \sigma_2 N + h.c. \right) \\ & - \frac{g_s}{2} \left( s_a^\dagger N^T \sigma_2 \tau_a \tau_2 N + h.c. \right) - G_3 N^\dagger \left[ g_t^2 (t_i \sigma_i)^\dagger (t_j \sigma_j) \right. \\ & \left. + \frac{g_t g_s}{3} \left( (t_i \sigma_i)^\dagger (s_a \tau_a) + h.c. \right) + g_s^2 (s_a \tau_a)^\dagger (s_b \tau_b) \right] N + \dots, \end{aligned} \quad (38)$$

where  $i, j$  are spin and  $a, b$  are isospin indices while  $g_t, g_s, \Delta_t, \Delta_s$  and  $G_3$  are the bare coupling constants. The Pauli matrices  $\sigma_i$  ( $\tau_a$ ) operate in spin (isospin) space, respectively. This Lagrangian goes beyond leading order and already includes the effective range terms. The coupling constants  $g_t, \Delta_t, g_s, \Delta_s$  are matched to the scattering lengths  $a_\alpha$  and effective ranges  $r_{0\alpha}$  in the two channels ( $\alpha = s, t$ ). Alternatively, one can match to the position of the bound state/virtual state pole  $\gamma_\alpha$  in the  $T$ -matrix instead of the scattering length which often improves convergence [59].

The term proportional to  $G_3$  constitutes a Wigner- $SU(4)$  symmetric three-body interaction. It only contributes in the spin-doublet S-wave channel. When the auxiliary dimeron fields  $t_i$  and  $s_a$  are integrated out, an equivalent form containing only nucleon fields is obtained. At leading order when the effective range corrections are neglected, the spatial and time derivatives acting on the dimeron fields are omitted and the field is static. The coupling constants  $g_\alpha$  and  $\Delta_\alpha$ ,  $\alpha = s, t$  are then not independent and only the combination  $g_\alpha^2/\Delta_\alpha$  enters in observables. This combination can then be matched to the scattering length or pole position.

The simplest three-body process to consider is neutron-deuteron scattering below the breakup threshold. In order to focus on the main aspects of renor-

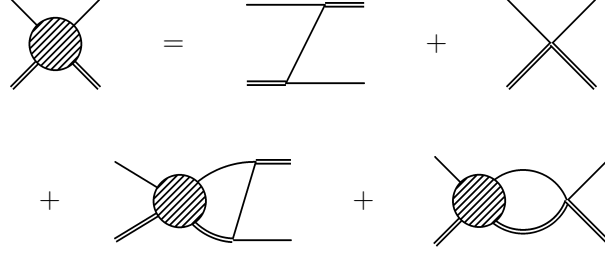


Figure 4: The integral equation for the particle-dimeron scattering amplitude. The single (double) line indicates the particle (dimeron) propagator.

malization, we suppress all spin-isospin indices and complications from coupled channels in the three-nucleon problem. This is equivalent to a system of three spinless bosons with large scattering length. If the scattering length is positive, the particles form a two-body bound state analog to the deuteron which we generically call dimeron. The leading order integral equation for particle-dimeron scattering is shown schematically in Fig. 4. Projected on total orbital angular momentum  $L = 0$ , it takes the following form:

$$T_3(k, p; E) = \frac{16}{3a} M(k, p; E) + \frac{4}{\pi} \int_0^\Lambda dq q^2 T_3(k, q; E) \times \frac{M(q, p; E)}{-1/a + \sqrt{3q^2/4 - mE - i\epsilon}}, \quad (39)$$

where the inhomogeneous term reads

$$M(k, p; E) = \frac{1}{2kp} \ln \left( \frac{k^2 + kp + p^2 - mE}{k^2 - kp + p^2 - mE} \right) + \frac{H(\Lambda)}{\Lambda^2}. \quad (40)$$

Here,  $H(\Lambda)$  is a running coupling constant that determines the strength of the three-body force  $G_3(\Lambda) = 2mH(\Lambda)/\Lambda^2$  and  $\Lambda$  is a UV cutoff introduced to regularize the integral equation. Note that the three-body force is enhanced and enters already at leading order in this theory. The magnitude of the incoming (outgoing) relative momenta is  $k$  ( $p$ ) and  $E = 3k^2/(4m) - 1/(ma^2)$ . The on-shell point corresponds to  $k = p$  and the phase shift can be obtained via  $k \cot \delta = 1/T_3(k, k; E) + ik$ . For  $H \equiv 0$  and  $\Lambda \rightarrow \infty$ , Eq. (39) reduces to the STM equation of Skorniakov and Ter-Martirosian [8]. It is well known that the STM equation has no unique solution [9]. The regularized STM equation has a unique solution for any given (finite) value of the ultraviolet cutoff  $\Lambda$  but the solution strongly depends on the value of  $\Lambda$ . In the EFT framework, cutoff independence of the amplitude is achieved by an appropriate “running” of  $H(\Lambda)$  [29, 60]:

$$H(\Lambda) = \frac{\cos[s_0 \ln(\Lambda/\Lambda_*) + \arctan s_0]}{\cos[s_0 \ln(\Lambda/\Lambda_*) - \arctan s_0]}, \quad (41)$$

where  $\Lambda_*$  is a dimensionful three-body parameter generated by dimensional transmutation. The dependence of the three-body coupling  $H$  on the cutoff  $\Lambda$  is shown

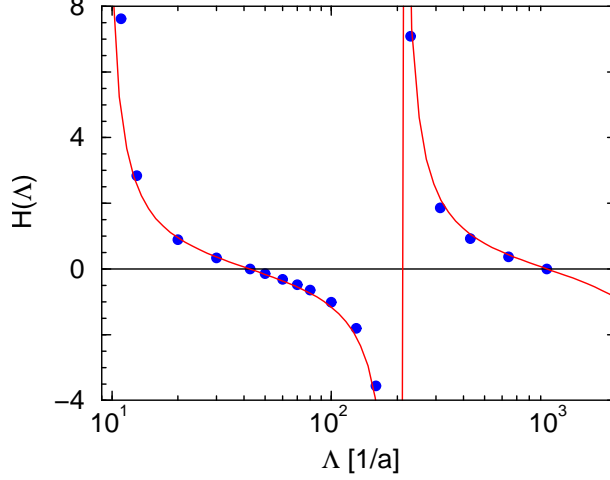


Figure 5: The three-body coupling  $H$  as a function of the cutoff  $\Lambda$  for a fixed value of the three-body parameter  $\Lambda_*$ . The solid line shows the analytical expression (41), while the dots show results from the numerical solution of Eq. (39).

in Fig. 5 for a fixed value of the three-body parameter  $\Lambda_*$ . The solid line shows the analytical expression (41), while the dots show results from the numerical solution of Eq. (39). A good agreement between both methods is observed, indicating that the renormalization is well under control. Adjusting  $\Lambda_*$  to a single three-body observable allows to determine all other low-energy properties of the three-body system.<sup>#1</sup> Because  $H(\Lambda)$  in Eq. (41) vanishes for certain values of the cutoff  $\Lambda$  it is possible to eliminate the explicit three-body force from the equations by working with a fixed cutoff that encodes the dependence on  $\Lambda_*$ . This justifies tuning the cutoff  $\Lambda$  in the STM equation to reproduce a three-body datum and using the same cutoff to calculate other observables as suggested by Kharchenko [61]. Equivalently, a subtraction can be performed in the integral equation [62, 63]. In all cases one three-body input parameter is needed for the calculation of observables.

The discrete scaling symmetry of the Efimov spectrum is manifest in the running of the coupling  $H(\Lambda)$ . The spectrum of three-body bound states of this EFT is exactly the Efimov spectrum. The integral equations for the three-nucleon problem derived from the Lagrangian (38) are a generalization of Eq. (39). (For

<sup>#1</sup>Note that the choice of the three-body parameter  $\Lambda_*$  is not unique, for alternative definitions see [1].

their explicit form and derivation, see e.g. Ref. [64].)

For S-wave nucleon-deuteron scattering in the spin-quartet channel only the spin-1 dimeron field contributes and the integral equation becomes [8, 21, 22]

$$T_3^{(3/2)}(p, k; E) = -\frac{4\gamma_t}{3}K(p, k) - \frac{1}{\pi} \int_0^\infty dq q^2 D_t(q; E) K(p, q) T_3^{(3/2)}(q, k; E) , \quad (42)$$

where

$$K(p, k) = \frac{1}{pk} \ln \left( \frac{p^2 + pk + k^2 - mE}{p^2 - pk + k^2 - mE} \right) , \quad (43)$$

$D_t(q; E)$  is the full spin-1 dimeron propagator and  $\gamma_t \approx 45$  MeV the deuteron pole momentum. This integral equation has a unique solution for  $\Lambda \rightarrow \infty$  and there is no three-body force in the first few orders. An S-wave three-body force is forbidden by the Pauli principle in this channel since all nucleon spins have to be aligned to obtain  $J = 3/2$ . The spin-quartet scattering phases  $k \cot \delta^{(3/2)} = 1/T_3^{(3/2)}(k, k; E) + ik$  can therefore be predicted to high precision from two-body data alone.

In the spin-doublet channel both dimeron fields as well as the three-body force in the Lagrangian (38) contribute [23]. This leads to a pair of coupled integral equations for the T-matrix. The renormalization of this equation is easily understood in the unitary limit which corresponds to a Wigner  $SU(4)$  symmetry of the theory [24]. In the unitary limit these two integral equations decouple. One of the two equations has the same structure as the equation for the bosonic problem (39), while the other one is similar to the equation in the quartet channel (42). Thus, one needs one new parameter which is not determined in the 2N system in order to fix the (leading) low-energy behavior of the 3N system in this channel. This parameter corresponds to the  $SU(4)$  symmetric three-body force proportional to  $G_3$  in the Lagrangian (38) [23]. The three-body parameter gives a natural explanation of universal correlations between different three-body observables such as the Phillips line, a correlation between the triton binding energy and the spin-doublet neutron-deuteron scattering length [31]. These correlations are purely driven by the large scattering length independent of the mechanism responsible for it. If the spin-doublet neutron-deuteron scattering length is given, the triton binding energy is predicted. In this scenario the triton emerges as an Efimov state. The scenario can be tested by using the effective theory to predict other three-body observables.

Higher-order corrections to the amplitude including the ones due to 2N effective range terms can be included perturbatively. This was first done at NLO

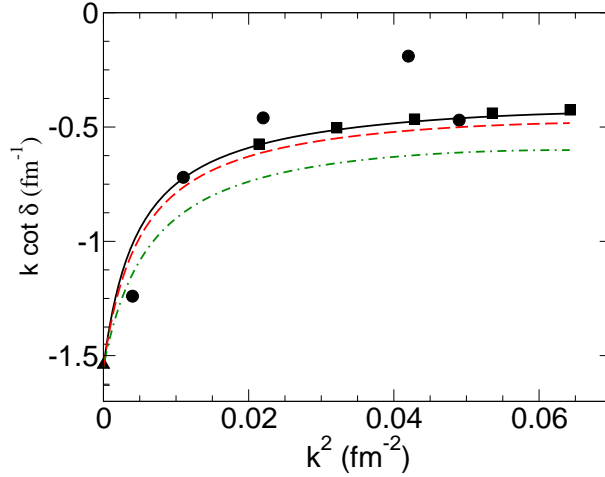


Figure 6: Phase shifts for neutron-deuteron scattering below the deuteron breakup at LO (dash-dotted line), NLO (dashed line), and N<sup>2</sup>LO (solid line). The filled squares and circles give the results of a phase shift analysis and a calculation using AV18 and the Urbana IX three-body force, respectively.

for the scattering length and triton binding energy in [20] and for the energy dependence of the phase shifts in [62]. In Refs. [64,65], it was demonstrated that it is convenient to iterate certain higher order range terms in order to extend the calculation to N<sup>2</sup>LO. Here, also a subleading three-body force was included as required by dimensional analysis. More recently, Platter and Phillips showed using the subtractive renormalization that the leading three-body force is sufficient to achieve cutoff independence up to N<sup>2</sup>LO in the expansion in  $M_{low}/M_{high}$  [66]. The results for the spin-doublet neutron-deuteron scattering phase shift at LO [23], NLO [62], and N<sup>2</sup>LO [67] are shown in Fig. 6. There is excellent agreement with the available phase shift analysis and a calculation using a phenomenological NN interaction. From dimensional analysis, one would expect the subleading three-body force at N<sup>2</sup>LO. Whether there is a suppression of the subleading three-body force or simply a correlation between the leading and subleading contributions is not understood.

Three-nucleon channels with higher orbital angular momentum are similar to the spin-quartet for S-waves and three-body forces do not appear until very high orders [68]. A general counting scheme for three-body forces based on the asymptotic behavior of the solutions of the leading order STM equation was proposed by Grieshammer [69]. A complementary approach to the few-nucleon problem is given by the renormalization group where the power counting is determined from the scaling of operators under the renormalization group transformation [70]. This method leads to consistent results for the power counting [71–73].

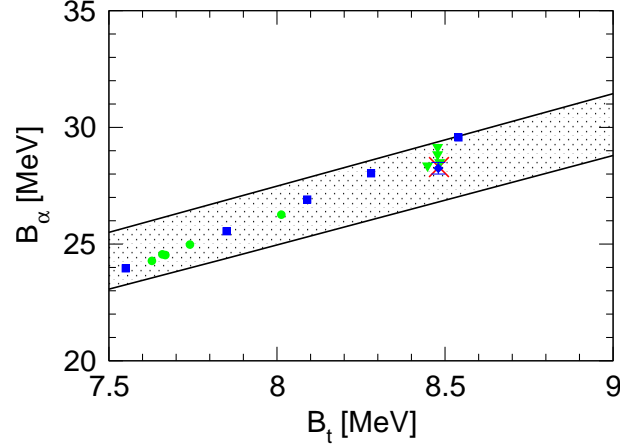


Figure 7: The Tjon line correlation as predicted by the pionless theory. The grey circles and triangles show various calculations using phenomenological potentials [81]. The squares show the results of chiral EFT at NLO for different cutoffs while the diamond gives the N<sup>2</sup>LO result [82, 83]. The cross shows the experimental point.

Three-body calculations with external currents are still in their infancy. However, a few exploratory calculations have been carried out. Universal properties of the triton charge form factor were investigated in Ref. [74] and neutron-deuteron radiative capture was calculated in Refs. [75–77]. Electromagnetic properties of the triton were recently investigated in Refs. [78, 79]. This work opens the possibility to carry out accurate calculations of electroweak reactions at very low energies for astrophysical processes.

The pionless approach has also been extended to the four-body sector [32, 80]. In order to be able to apply the Yakubovsky equations, an equivalent effective quantum mechanics formulation was used. The study of the cutoff dependence of the four-body binding energies revealed that no four-body parameter is required for renormalization at leading order. As a consequence, there are universal correlations in the four-body sector which are also driven by the large scattering length. The best known example is the Tjon line: a correlation between the triton and alpha particle binding energies,  $B_t$  and  $B_\alpha$ , respectively. Of course, higher order corrections break the exact correlation and generate a band. In Fig. 7, we show this band together with some calculations using phenomenological potentials [81] and a chiral EFT potential with explicit pions [82, 83]. All calculations with interactions that give a large scattering length must lie within the band. Different short-distance physics and/or cutoff dependence should only move the results along the band. This can for example be observed in the NLO results with the chiral potential indicated by the squares in Fig. 7 or in the few-body calculations



with the low-momentum NN potential  $V_{\text{low } k}$  carried out in Ref. [84]. The  $V_{\text{low } k}$  potential is obtained from phenomenological NN interactions by integrating out high-momentum modes above a cutoff  $\Lambda$  but leaving two-body observables (such as the large scattering lengths) unchanged. The results of few-body calculations with  $V_{\text{low } k}$  are not independent of  $\Lambda$  but lie all close to the Tjon line (cf. Fig. 2 in Ref. [84]).

Another interesting development is the application of the Resonating Group Model to solve the pionless EFT for three- and four-nucleon systems [85]. This method allows for a straightforward inclusion of Coulomb effects. Kirscher et al. extended previous calculations in the four-nucleon system to next-to-leading order and showed that the Tjon line correlation persists. Moreover, they calculated the correlation between the singlet S-wave  $^3\text{He}$ -neutron scattering length and the triton binding energy. Preliminary results for the halo nucleus  $^6\text{He}$  have been reported in [86].

The pionless theory has also been applied within the no-core shell model approach. Here the expansion in a truncated harmonic oscillator basis is used as the ultraviolet regulator of the EFT. The effective interaction is determined directly in the model space, where an exact diagonalization in a complete many-body basis is performed. In Ref. [87], the  $0^+$  excited state of  $^4\text{He}$  and the  $^6\text{Li}$  ground state were calculated using the deuteron, triton, alpha particle ground states as input. The first  $0^+$  excited state in  $^4\text{He}$  is calculated within 10% of the experimental value, while the  $^6\text{Li}$  ground state comes out at about 70% of the experimental value in agreement with the 30 % error expected for the leading order approximation. These results are promising and should be improved if range corrections are included. Finally, the spectrum of trapped three- and four-fermion systems was calculated using the same method [88]. In this case the harmonic potential is physical and not simply used as an ultraviolet regulator. For an update on this work, see [89].

### 3.2 Quark Mass Dependence and Infrared Limit Cycle

In the following, we discuss the possibility of an exact infrared limit cycle and the Efimov effect in a deformed version of QCD with quark masses slightly larger than their physical values. The quark mass dependence of the chiral NN interaction was calculated to next-to-leading order (NLO) in the chiral counting in Refs. [90, 91]. At this order, the quark mass dependence is synonymous to the pion mass

dependence because of the Gell-Mann-Oakes-Renner relation:  $M_\pi^2 = -(m_u + m_d)\langle 0|\bar{u}u|0\rangle/F_\pi^2$ , where  $\langle 0|\bar{u}u|0\rangle \approx (-290 \text{ MeV})^3$  is the quark condensate. In the following, we will therefore refer to the pion mass dependence instead of the quark mass dependence which is more convenient for our purpose. The pion mass dependence of the nucleon-nucleon scattering lengths in the  $^3S_1$ - $^3D_1$  and  $^1S_0$  channels as well as the deuteron binding energy were calculated in Refs. [90–92].

In principle, the pion mass dependence of the chiral NN potential is determined uniquely. However, the extrapolation away from the physical pion mass generates errors. The dominating source are the constants  $\bar{C}_{S,T}$  and  $\bar{D}_{S,T}$  which give the corrections to the LO contact terms  $\propto M_\pi^2$  and cannot be determined independently from fits to data at the physical pion mass. A smaller effect is due to the error in the LEC  $\bar{d}_{16}$ , which governs the pion mass dependence of  $g_A$ . Both effects generate increasing uncertainties as one extrapolates away from the physical point.

In the calculation of Ref. [91], the size of the two constants  $\bar{D}_S$  and  $\bar{D}_T$  was constrained from naturalness arguments, assuming  $-3 \leq F_\pi^2 \Lambda_\chi^2 \bar{D}_{S,T} \leq 3$ , where  $\Lambda_\chi \simeq 1 \text{ GeV}$  is the chiral symmetry breaking scale. These bounds are in agreement with resonance saturation estimates [93]. The constant  $\bar{d}_{16}$  was varied in the range  $\bar{d}_{16} = -0.91 \dots -1.76 \text{ GeV}^{-2}$  [94]. These ranges were used to estimate the extrapolation errors of two-nucleon observables like the deuteron binding energy and the spin-singlet and spin-triplet scattering lengths [91]. In the chiral limit the deuteron binding energy was found to be of natural size,  $B_d \sim F_\pi^2/m \simeq 10 \text{ MeV}$ . Note, however, that if larger uncertainties in the LECs  $\bar{D}_S$  and  $\bar{D}_T$  are assumed one cannot make a definite statement about the binding of the deuteron in the chiral limit [90, 92]. For pion masses above the physical value, however, all calculations show similar behavior.

In Fig. 8, we show the inverse scattering lengths in the spin-triplet and spin-singlet channels from Ref. [91] together with some recent lattice results [97]. Figure 8 also shows that a scenario where both inverse scattering lengths vanish simultaneously at a critical pion mass of about 200 MeV is possible. For pion masses below the critical value, the spin-triplet scattering length is positive and the deuteron is bound. As the inverse spin-triplet scattering length decreases, the deuteron becomes more and more shallow and finally becomes unbound at the critical mass. Above the critical pion mass the deuteron exists as a shallow virtual state. In the spin-singlet channel, the situation is reversed: the “spin-singlet deuteron” is a virtual state below the critical pion mass and becomes bound

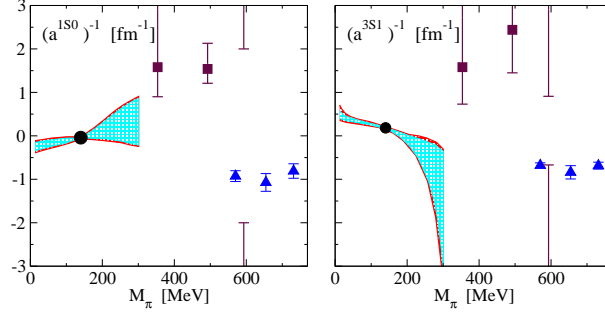


Figure 8: Inverse of the S-wave scattering lengths in the spin-triplet and spin-singlet nucleon-nucleon channels as a function of the pion mass  $M_\pi$ . Filled triangles and rectangles show the lattice calculations from Refs. [95, 96] and [97], respectively.

above. Based on this behavior Braaten and Hammer conjectured that one should be able to reach the critical point by varying the up- and down-quark masses  $m_u$  and  $m_d$  independently because the spin-triplet and spin-singlet channels have different isospin [54]. In this case, the triton would display the Efimov effect which corresponds to the occurrence of an infrared limit cycle in QCD. It is evident that a complete investigation of this issue requires the inclusion of isospin breaking corrections and therefore higher orders in the chiral EFT. However, the universal properties of the limit cycle have been investigated by considering specific values of  $\bar{D}_S$  and  $\bar{D}_T$  that lie within the naturalness bound and cause the spin-singlet and spin-triplet scattering lengths to become infinite at the same value of the pion mass.

In Ref. [98], the properties of the triton around the critical pion mass were studied for one particular solution with a critical pion mass  $M_\pi^{crit} = 197.8577$  MeV. From the solution of the Faddeev equations, the binding energies of the triton and the first two excited states in the vicinity of the limit cycle were calculated for this scenario in chiral EFT. The binding energies are given in Fig. 9 by the circles (ground state), squares (first excited state), and diamonds (second excited state). The dashed lines indicate the neutron-deuteron ( $M_\pi \leq M_\pi^{crit}$ ) and neutron-spin-singlet-deuteron ( $M_\pi \geq M_\pi^{crit}$ ) thresholds where the three-body states become unstable. Directly at the critical mass, these thresholds coincide with the three-body threshold and the triton has infinitely many excited states. The solid lines are leading order calculations in the pionless theory using the pion mass dependence of the nucleon-nucleon scattering lengths and one triton state from chiral EFT as input. The chiral EFT results for the other triton states in the critical region are reproduced very well. The binding energy of the triton

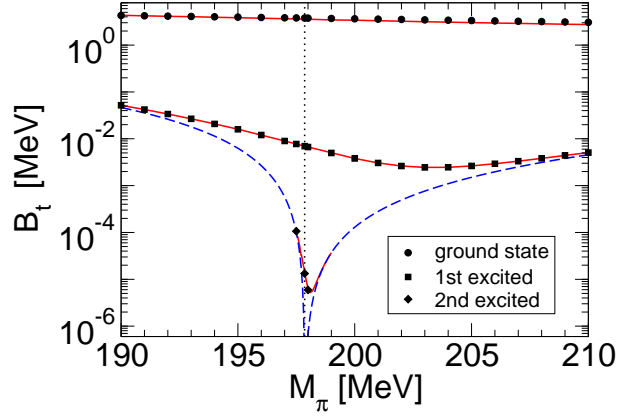


Figure 9: Binding energies  $B_t$  of the triton ground and first two excited states as a function of  $M_\pi$ . The circles, squares, and diamonds give the chiral EFT result, while the solid lines are calculations in the pionless theory. The vertical dotted line indicates the critical pion mass  $M_\pi^{crit}$  and the dashed lines are the bound state thresholds.

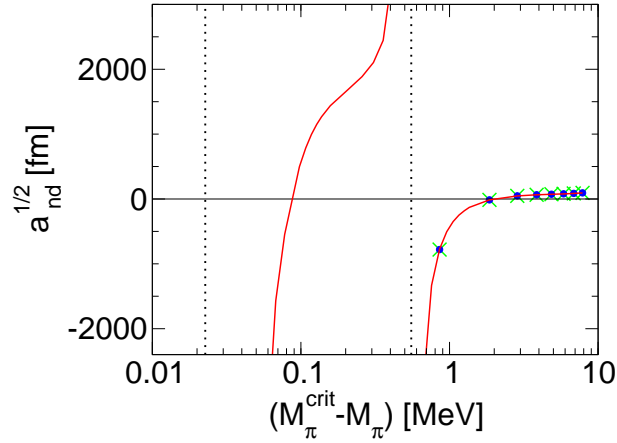


Figure 10: Doublet neutron-deuteron scattering length  $a_{nd}^{1/2}$  in the critical region computed in the pionless EFT. The solid line gives the LO result, while the crosses and circles show the NLO and N<sup>2</sup>LO results. The dotted lines indicate the pion masses at which  $a_{nd}^{1/2}$  diverges.

ground state varies only weakly over the whole range of pion masses and is about one half of the physical value at the critical point. The excited states are strongly influenced by the thresholds and vary much more strongly.

These studies were extended to N<sup>2</sup>LO in the pionless EFT and neutron-deuteron scattering observables in Ref. [99]. It was demonstrated that the higher order corrections in the vicinity of the critical pion mass are small. This is illustrated in Fig. 10, where we show the doublet scattering length  $a_{nd}^{1/2}$  in the critical region. The solid line gives the LO result, while the crosses and circles show the NLO and N<sup>2</sup>LO results. The dotted lines indicate the pion masses at which  $a_{nd}^{1/2}$  di-

verges because the second and third excited states of the triton appear at the neutron-deuteron threshold. These singularities in  $a_{nd}^{1/2}(M_\pi)$  are a clear signature that the limit cycle is approached in the critical region.

A final answer on the question of whether an infrared limit cycle can be realized in QCD can only be given by solving QCD directly. In particular, it would be very interesting to know whether this can be achieved by appropriately tuning the quark masses in a Lattice QCD simulation [100]. The first full lattice QCD calculation of nucleon-nucleon scattering was reported in [97] but statistical noise presented a serious challenge. A promising recent high-statistics study of three-baryon systems presented also initial results for a system with the quantum numbers of the triton such that lattice QCD calculations of three-nucleon systems are now within sight [101]. For a review of these activities, see Ref. [102]. Such calculations require a detailed understanding of the modification of the Efimov spectrum in a cubic box. For identical bosons, there are significant finite volume shifts even for moderate box sizes [103]. These shifts show universal scaling behavior which could be exploited to reduce the computational effort [104]. The extension of these studies to the triton case is in progress.

### 3.3 Halo Nuclei

A special class of nuclear systems exhibiting universal behavior are *halo nuclei* [27, 105]. Halo nuclei consist of a tightly bound core surrounded by one or more loosely bound valence nucleons. The valence nucleons are characterized by a very low separation energy compared to those in the core. As a consequence, the radius of the halo nucleus is large compared to the radius of the core. A trivial example is the deuteron, which can be considered a two-body halo nucleus. The root mean square radius of the deuteron is about three times larger than the size of the constituent nucleons. Halo nuclei with two valence nucleons are particularly interesting examples of three-body systems. If none of the two-body subsystems are bound, they are called *Borromean* halo nuclei. This name is derived from the heraldic symbol of the Borromeo family of Italy, which consists of three rings interlocked in such way that if any one of the rings is removed the other two separate. The most carefully studied Borromean halo nuclei are  ${}^6\text{He}$  and  ${}^{11}\text{Li}$ , which have two weakly bound valence neutrons [105]. In the case of  ${}^6\text{He}$ , the core is a  ${}^4\text{He}$  nucleus, which is also known as the  $\alpha$  particle. The two-neutron separation energy for  ${}^6\text{He}$  is about 1 MeV, small compared to the binding energy

of the  $\alpha$  particle which is about 28 MeV. The neutron- $\alpha$  ( $n\alpha$ ) system has no bound states and the  ${}^6\text{He}$  nucleus is therefore Borromean. There is, however, a strong P-wave resonance in the  $J = 3/2$  channel of  $n\alpha$  scattering which is sometimes referred to as  ${}^5\text{He}$ . This resonance is responsible for the binding of  ${}^6\text{He}$ . Thus  ${}^6\text{He}$  can be interpreted as a bound state of an  $\alpha$ -particle and two neutrons, both of which are in  $P_{3/2}$  configurations.

Because of the separation of scales in halo nuclei, they can be described by extensions of the pionless EFT. One can assume the core to be structureless and treats the nucleus as a few-body system of the core and the valence nucleons. Corrections from the structure of the core appear in higher orders and can be included in perturbation theory. Cluster models of halo nuclei then appear as leading order approximations in this “halo EFT”. A new facet is the appearance of resonances as in the neutron-alpha system which leads to a more complicated singularity structure and renormalization compared to the few-nucleon system discussed above [106].

The first application of effective field theory methods to halo nuclei was carried out in Refs. [106, 107], where the  $n\alpha$  system (“ ${}^5\text{He}$ ”) was considered. It was found that for resonant P-wave interactions both the scattering length and effective range have to be resummed at leading order. At threshold, however, only one combination of coupling constants is fine-tuned and the EFT becomes perturbative. Because the  $n\alpha$  interaction is resonant in the P-wave and not in the S-wave, the binding mechanism of  ${}^6\text{He}$  is not the Efimov effect. However, this nucleus can serve as a laboratory for studying the interplay of resonance structures in higher partial waves.

Three-body halo nuclei composed of a core and two valence neutrons are of particular interest due to the possibility of these systems to display the Efimov effect [3]. Since the scattering length can not easily be varied in halo nuclei, one looks for Efimov scaling between different states of the same nucleus. Such analyses assume that the halo ground state is an Efimov state.<sup>#2</sup> They have previously been carried out in cluster models and the renormalized zero-range model (See, e.g. Refs. [108–110]). A comprehensive study of S-wave halo nuclei in halo EFT was recently carried out in Ref. [111]. This work provided binding energy and structure calculations for various halo nuclei including error estimates. Confirming earlier results by Fedorov et al. [108] and Amorim et al. [109],  ${}^{20}\text{C}$  was

---

<sup>#2</sup>We note that it is also possible that only the excited state is an Efimov state while the ground state is more compact. This scenario can not be ruled out but is also less predictive.

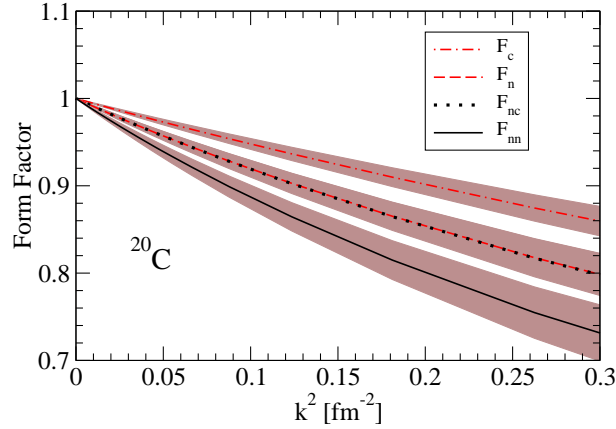


Figure 11: The one- and two-body matter density form factors  $\mathcal{F}_c$ ,  $\mathcal{F}_n$ ,  $\mathcal{F}_{nc}$ , and  $\mathcal{F}_{nn}$  with leading order error bands for the ground state of  $^{20}\text{C}$  as a function of the momentum transfer  $k^2$ .

found to be the only candidate nucleus for an excited Efimov state assuming the ground state is also an Efimov state. This nucleus consists of a  $^{18}\text{C}$  core with spin and parity quantum numbers  $J^P = 0^+$  and two valence neutrons. The nucleus  $^{19}\text{C}$  is expected to have a  $\frac{1}{2}^+$  state near threshold, implying a shallow neutron-core bound state and therefore a large neutron-core scattering length. The value of the  $^{19}\text{C}$  energy, however, is not known well enough to make a definite statement about the appearance of an excited state in  $^{20}\text{C}$ . An excited state with a binding energy of about 65 keV is marginally consistent with the current experimental information.

The matter form factors and radii of halo nuclei can also be calculated in the halo EFT [111, 112]. As an example, we show the various one- and two-body matter density form factors  $\mathcal{F}_c$ ,  $\mathcal{F}_n$ ,  $\mathcal{F}_{nc}$ , and  $\mathcal{F}_{nn}$  with leading order error bands for the ground state of  $^{20}\text{C}$  as a function the momentum transfer  $k^2$  from [111] in Fig. 11. The theory breaks down for momentum transfers of the order of the pion-mass squared ( $k^2 \approx 0.5 \text{ fm}^{-2}$ ).

From the slope of the matter form factors one can extract the corresponding radii:

$$\mathcal{F}(k^2) = 1 - \frac{1}{6}k^2 \langle r^2 \rangle + \dots \quad (44)$$

Information on these radii has been extracted from experiment for some halo nuclei based on intensity interferometry and Dalitz plots [113]. Within the error estimates, the extracted values are in good agreement with the theoretical predictions from halo EFT [111]. For the possible  $^{20}\text{C}$  excited state, the halo EFT at leading order predicts neutron-neutron and neutron-core radii of order

40 fm while the ground state radii are of order 2-3 fm. The theoretical errors are estimated to be of order 10%. Assuming a natural value for the effective range of the  $n$ - $^{18}\text{C}$  interaction,  $r_0 \approx 1/M_\pi$ , next-to-leading order predictions for these radii have recently been obtained [114]. The leading order results were found to be stable under inclusion of the leading effective range corrections and the typical errors could be reduced to about 1-2%.

Scattering observables offer a complementary window on Efimov physics in halo nuclei and some recent model studies have focused on this issue. In particular, in Refs. [115,116] the trajectory of the possible  $^{20}\text{C}$  excited state was extended into the scattering region in order to find a resonance in  $n$ - $^{19}\text{C}$  scattering. A detailed study of  $n$ - $^{19}\text{C}$  scattering near an Efimov state was carried out in [117].

The simplest strange halo nucleus is the hypertriton, a three-body bound state of a proton, neutron and the  $\Lambda$ . The total binding energy is only about 2.4 MeV. The separation energy for the  $\Lambda$ ,  $E_\Lambda = 0.13$  MeV, is tiny compared to the binding energy  $B_d = 2.22$  MeV of the deuteron. The hypertriton can therefore also be considered a two-body halo nucleus. It has been studied in both two-body and three-body approaches [118–120]. A study of the hypertriton in the halo EFT was carried out in Ref. [121]. The  $\Lambda N$  scattering lengths are not well known experimentally since the few scattering data are at relatively high energies. If the  $\Lambda N$  scattering lengths are large, the hypertriton is likely bound due to the Efimov effect. In this case there will also be a correlation between the  $\Lambda d$  scattering length  $a_{\Lambda d}$  and the hypertriton binding energy  $B_t^\Lambda$  analog to the Phillips line in the neutron-deuteron system [119]. In Fig. 12, we show this Phillips line correlation for three values of the  $\Lambda N$  pole position  $\gamma_i$  [121]. For small hypertriton energies  $B_t^\Lambda$ , the different Phillips lines coincide exactly (the physical hypertriton corresponds to  $MB_t^\Lambda \approx 1.06 \gamma_t^2$ ) and deviate from each other only at very large binding energies where the EFT breaks down. For all practical purposes the Phillips line is therefore independent of  $\gamma_i$ . Whether the Efimov effect plays a role for the hypertriton is an open question. Most modern hyperon-nucleon potentials, however, favor a natural  $\Lambda N$  scattering length [52].

Another powerful method that can be used to investigate the Efimov effect in three-body halo nuclei at existing and future facilities with exotic beams (such as FAIR and FRIB) is Coulomb excitation. In these experiments a nuclear beam scatters off the Coulomb field of a heavy nucleus. Such processes can populate excited states of the projectile which subsequently decay, leading to its “Coulomb dissociation” [122]. The halo EFT offers a systematic framework for a



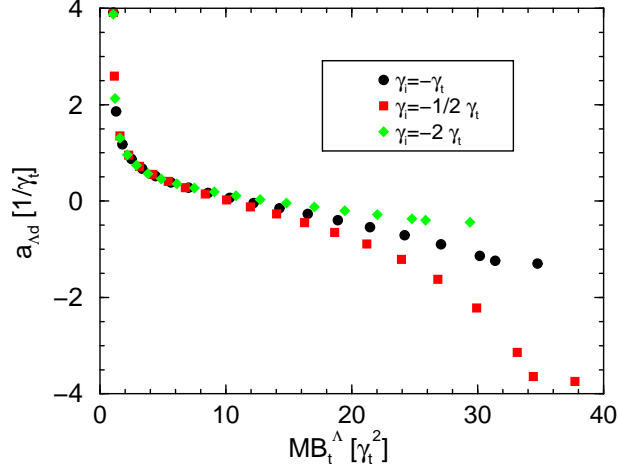


Figure 12: Phillips line in the hypertriton channel for different values of the  $\Lambda N$  pole position  $\gamma_i$  (all quantities are in units of the deuteron pole position  $\gamma_t \approx 45$  MeV).

full quantum-mechanical treatment and can be used to predict the signature of the Efimov effect in these reactions.

### 3.4 Three-Alpha System and Coulomb Interaction

The excited  $0^+$  state in  $^{12}\text{C}$  is known as the Hoyle state. Its properties are important for stellar astrophysics since it determines the ratio of carbon to oxygen in stellar helium burning. Efimov suggested that the Hoyle state could be explained as an Efimov state of  $\alpha$  particles [3, 17]. (For a more detailed discussion, see Ref. [123].) In this case, the universal properties are modified by the long-range Coulomb interaction. The modified Efimov spectrum needs to be understood before any definite statement about the nature of the Hoyle state can be made.

Many recent studies have focused on the consistent inclusion of the Coulomb interaction in two-body halo nuclei such as the  $p\alpha$  and  $\alpha\alpha$  systems [124, 125]. In particular, the  $\alpha\alpha$  system shows a surprising amount of fine-tuning between the strong and electromagnetic interaction. It can be understood in an expansion around the limit where, when electromagnetic interactions are turned off, the  $^8\text{Be}$  ground state is exactly at threshold and exhibits conformal invariance [125]. In this scenario, the Hoyle state in  $^{12}\text{C}$  would indeed appear as a remnant of an excited Efimov state. In order to better understand the modification of the Efimov spectrum and limit cycles by long-range interactions such as the Coulomb interaction, a one dimensional inverse square potential supplemented with a Coulomb interaction was investigated in [126]. The results indicate that the counterterm

required to renormalize the inverse square potential alone is sufficient to renormalize the full problem. However, the breaking of the discrete scale invariance through the Coulomb interaction leads to a modified bound state spectrum. The shallow bound states are strongly influenced by the Coulomb interaction while the deep bound states are dominated by the inverse square potential. These results support the conjecture of the Hoyle state being an Efimov state of  $\alpha$  particles but a full calculation of the  $3\alpha$  system including Coulomb in the halo EFT is missing. Calculations with the fermionic molecular dynamics model and electron scattering data, however, support a pronounced  $\alpha$  cluster structure of the Hoyle state [127].

## 4 Applications in Particle Physics

### 4.1 Hadronic Molecules

In recent years many new and possibly exotic charmonium states have been observed at the B-factories at SLAC, at KEK in Japan, and at the CESR collider at Cornell. This has revived the field of charmonium spectroscopy [128–130]. Several of the new states exist very close to scattering thresholds, and can be interpreted as hadronic molecules. If they are sufficiently shallow, one may ask whether there are any three-body hadronic molecules bound by the Efimov effect.

A particularly interesting example is the  $X(3872)$ , discovered by the Belle collaboration [131] in  $B^\pm \rightarrow K^\pm \pi^+ \pi^- J/\psi$  decays and quickly confirmed by CDF [132], D0 [133], and BaBar [134]. The state has likely quantum numbers  $J^{PC} = 1^{++}$  and is very close to the  $D^{*0} \bar{D}^0$  threshold. As a consequence, the  $X(3872)$  has a resonant S-wave coupling to the  $D^{*0} \bar{D}^0$  system. An extensive program provides predictions for its decay modes based on the assumption that it is a  $D^{*0} \bar{D}^0$  molecule with even C-parity:

$$(D^{*0} \bar{D}^0)_+ \equiv \frac{1}{\sqrt{2}} (D^{*0} \bar{D}^0 + D^0 \bar{D}^{*0}) . \quad (45)$$

This assumption naturally explains several puzzling features such the apparently different mass in the  $J/\psi \pi^+ \pi^-$  and  $D^{*0} \bar{D}^0$  decay channels and the isospin violating decays [135, 136]. A status report with references to the original literature can be found in Ref. [137].

Using the latest measurements in the  $J/\psi \pi^+ \pi^-$  channel, the mass of the  $X(3872)$  is [138]:  $m_X = (3871.55 \pm 0.20) \text{ MeV}$ , which corresponds to an energy

relative to the  $D^{*0}\bar{D}^0$  threshold of

$$E_X = (-0.26 \pm 0.41) \text{ MeV}. \quad (46)$$

The central value corresponds to a  $(D^{*0}\bar{D}^0)_+$  bound state with binding energy  $B_X = 0.26 \text{ MeV}$  (but a virtual state cannot be excluded from the current data in the  $J/\psi\pi^+\pi^-$  and  $D^{*0}\bar{D}^0$  channels [139–141]). The  $X(3872)$  is also very narrow, with a width smaller than 2.3 MeV.

Because the  $X(3872)$  is so close to the  $D^{*0}\bar{D}^0$  threshold, it has universal low-energy properties that depend only on its binding energy [142]. Close to threshold, the coupling to charged  $D$  mesons can be neglected because the  $D^{*+}\bar{D}^-$  threshold is about 8 MeV higher in energy. Therefore, the properties of the  $X(3872)$  can be described in a universal EFT with contact interactions only. Unfortunately, there is no Efimov effect in this system [142], so universal bound states of the  $X$  and  $D^0$  or  $D^{*0}$  mesons do not exist. The reason for this is that there is not a sufficient number of pairs with resonant interactions as only the  $D^{*0}\bar{D}^0$  and  $D^0\bar{D}^{*0}$  interactions are resonant. However, it is possible to provide model-independent predictions for the scattering of  $D^0$  and  $D^{*0}$  mesons and their antiparticles off the  $X(3872)$ . This scattering process is to leading order determined by the  $D^{*0}\bar{D}^0$  and  $D^0\bar{D}^{*0}$  interactions only.

The corresponding cross sections as a function of the center-of-mass momentum  $k$  obtained in [138] are shown in Fig. 13. The difference between the contribution of S-waves ( $L = 0$ ) and the full cross section (including all partial waves up to  $L = 6$ ) is negligible for momenta below the bound state pole momentum  $\gamma$ . Our results are given in units of the scattering length and may be scaled to physical units once  $a$  is determined. At present the error in the experimental value for  $E_X$  in Eq. (46) implies a large error in the scattering length. In particular, we obtain the ranges  $\gamma = (0 \dots 36) \text{ MeV}$  for the pole momentum and  $a = (5.5 \dots \infty) \text{ fm}$  for the scattering length with central values  $\gamma = 22 \text{ MeV}$  and  $a = 8.8 \text{ fm}$ . Using the central value of the scattering length, we obtain for the scale factor  $a^2 = 0.78 \text{ barn}$ . This factor can become infinite if the  $X(3872)$  is directly at threshold, while the lower bound from the error in  $E_X$  would give a value of 0.3 barn. Even in this case the total cross section at threshold will be of the order 300 barns for  $D^0X$  scattering and 1000 barns for  $D^{*0}X$  scattering. It may be possible to extract the scattering within the final state interactions of  $B_c$  decays and/or other LHC events. Observation of enhanced final state interactions would provide an independent confirmation of the nature of the  $X(3872)$ .

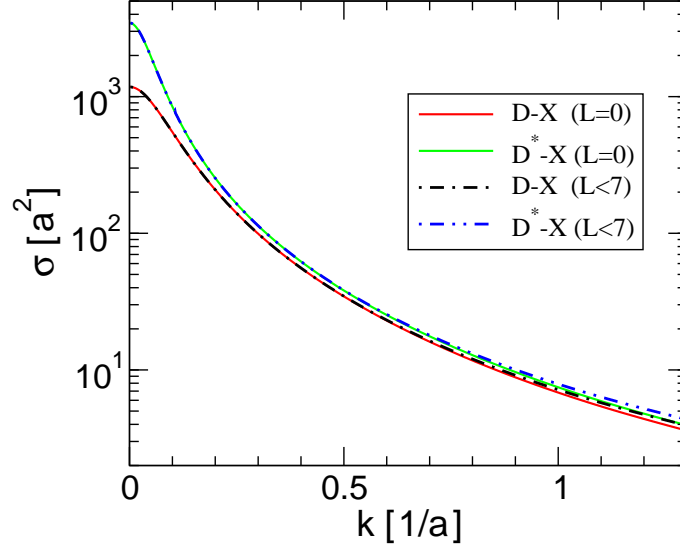


Figure 13: Total cross section for scattering of  $D^0$  and  $D^{*0}$  mesons off the  $X(3872)$  for S-waves ( $L = 0$ ) and including higher partial waves with  $L < 7$ , in units of the scattering length  $a$ . The cross section is the same for the scattering of particles as it is for the scattering of antiparticles.

There may also be hadronic three-body molecules that are bound due to the Efimov effect but currently no strong candidate states are known. This situation will be improved by new experiments at facilities such as FAIR and Belle II which have a dedicated program to study exotic charmonium states.

## 5 Summary and Outlook

Any few-body system with short-range interactions that has a two-body scattering length larger than the range of the underlying interaction will display universal properties and Efimov physics. This statement is independent of the typical length scale of the system and atomic, nuclear and particle physics can provide examples of universality. While much progress has been made recently in experiments with ultracold atoms, the concept of Efimov physics was originally devised for the few-nucleon problem. As we have shown, it can serve as a starting point for a description of very low-energy nuclear phenomena in an expansion around the unitary limit.

In this review we have discussed the manifestation of Efimov physics with a strong emphasis on nuclear and particle physics. There are a number of such systems that display low-energy universality associated with Efimov physics. The most important example from nuclear physics is the triton. The nucleon-nucleon

scattering length is large compared to the range of the internuclear interaction. Phase shift equivalent  $NN$  potentials will therefore necessarily give results for triton binding energy and neutron-deuteron scattering length that are correlated and lie on the Phillips line. The implications of universality on the four-nucleon system have been also been explored. It was found that the Tjon line, a correlation between three-nucleon and four-nucleon binding energies is a result of the large two-nucleon scattering length.

Halo nuclei might provide a further example of few-body universality. In particular two-neutron Halos such as  $^{20}\text{C}$  could display Efimov physics in form of an excited three-body state due to the large core-neutron scattering length. While first studies of bound state observables have become available, scattering calculations represent an exciting opportunity for future applications of the EFT approach. In particular so-called  $p - t$  reactions in which a triton is formed in a collision of a proton and a two-neutron halo will provide an important benchmark.

Several new charmonium states have recently been discovered close to scattering thresholds and can be interpreted as hadronic molecules. If they are sufficiently shallow, they have universal properties associated with large scattering length physics. The best known example is the  $X(3872)$  which may be interpreted as a  $D^{*0}\bar{D}^0$  molecule with even C-parity. There may also be three-body hadronic molecules bound by the Efimov effect but currently no strong candidates are known.

The separation of scales between scattering length and range facilitates the application of an EFT that reproduces at leading order the results obtained by Efimov and is known as the pionless EFT. Within this framework corrections to the zero-range limit can be calculated systematically in a small parameter expansion in powers of  $k\ell$  and  $\ell/a$ . The number of few-body calculations that include higher order corrections is growing. As a consequence, the expansion around the unitary limit provides a useful starting point for a controlled description of very low energy phenomena in nuclear and particle physics. The intricate consequences of Efimov physics are explicit in this framework and universal correlations between observables arise naturally. Moreover, this theory is an ideal tool to unravel universal properties and establish connections between different fields of physics.

The constituents of nuclear few-body systems can have charge in contrast to the neutral atoms used in experiments with ultracold gases. Electroweak observables provide thus additional information on few-body universality. However,

they are also of interest by themselves and the pionless EFT guarantees a consistent framework for the calculation of observables with the minimal number of parameters as it is straightforward to consider external currents in any EFT. First calculations for observables such as form factors and capture rates have been performed but many more remain to be calculated. Of very high interest are in this context thermal capture rates in the four-nucleon sector that are relevant to big bang nucleosynthesis.

## Acknowledgements

We thank Eric Braaten and Vitaly Efimov for discussions. This research was supported by the National Science Foundation under Grant No. PHY-0653312, by the UNEDF SciDAC Collaboration under DOE Grant DE-FC02-07ER41457, by the Department of Energy under grant number DE-FG02-00ER41132, by the Deutsche Forschungsgemeinschaft through SFB/TR16, and by the Bundesministerium für Bildung und Forschung under contracts 06BN411 and 06BN9006.

## LITERATURE CITED

1. E. Braaten and H. W. Hammer, Phys. Rept. **428**, 259 (2006), cond-mat/0410417.
2. L. Platter, Few Body Syst. **46** (2009).
3. V. Efimov, Phys. Lett. **B33**, 563 (1970).
4. W. Schöllkopf and J. Toennies, Science **266**, 1345 (1994).
5. T. Kraemer *et al.*, Nature **440** (2006).
6. E. Braaten and H. W. Hammer, Annals Phys. **322**, 120 (2007), cond-mat/0612123.
7. L. Thomas, Phys. Rev. **47**, 903 (1935).
8. G. V. Skorniakov and K. A. Ter-Martirosian, Sov. Phys. JETP **4**, 648 (1957).
9. G. Danilov, Sov. Phys. JETP **13**, 349 (1961).
10. L. D. Faddeev and R. A. Minlos, Sov. Phys. JETP **14**, 1315 (1962).
11. R. Minlos and L. Faddeev, Sov. Phys. Doklady **6**, 1072 (1962).
12. G. Danilov and V. Lebedev, Sov. Phys. JETP **17**, 1015 (1963).
13. R. D. Amado and J. V. Noble, Physics Letters B **35**, 25 (1971).
14. R. D. Amado and J. V. Noble, Phys. Rev. D **5**, 1992 (1972).

15. S. K. Adhikari, A. Delfino, T. Frederico, I. D. Goldman, and L. Tomio, *Phys. Rev. A* **37**, 3666 (1988).
16. S. Albeverio, R. Hegh-Krohn, and T. T. Wu, *Physics Letters A* **83**, 105 (1981).
17. V. N. Efimov, *Sov. J. Nucl. Phys.* **12**, 589 (1971).
18. V. Efimov, *Sov. J. Nucl. Phys.* **29**, 546 (1979).
19. V. Efimov, *Nucl. Phys.* **A362**, 45 (1981).
20. V. Efimov, *Phys. Rev.* **C44**, 2303 (1991).
21. P. F. Bedaque and U. van Kolck, *Phys. Lett. B* **428**, 221 (1998), [nucl-th/9710073](#).
22. P. F. Bedaque, H. W. Hammer, and U. van Kolck, *Phys. Rev. C* **58**, 641 (1998), [nucl-th/9802057](#).
23. P. F. Bedaque, H. W. Hammer, and U. van Kolck, *Nucl. Phys. A* **676**, 357 (2000), [nucl-th/9906032](#).
24. E. Wigner, *Phys. Rev.* **51**, 106 (1937).
25. T. Mehen, I. W. Stewart, and M. B. Wise, *Phys. Rev. Lett.* **83**, 931 (1999), [hep-ph/9902370](#).
26. E. Nielsen, D. Fedorov, A. Jensen, and E. Garrido, *Phys. Rep.* **347**, 373 (2001).
27. A. S. Jensen, K. Riisager, D. V. Fedorov, and E. Garrido, *Rev. Mod. Phys.* **76**, 215 (2004).
28. E. Braaten and D. Phillips, *Phys. Rev. A* **70** (2004), [hep-th/0403168](#).
29. P. F. Bedaque, H. W. Hammer, and U. van Kolck, *Phys. Rev. Lett.* **82**, 463 (1999), [nucl-th/9809025](#).
30. L. Platter, C. Ji, and D. R. Phillips, *Phys. Rev. A* **79** (2009).
31. A. Phillips, *Nucl. Phys.* **A107**, 209 (1968).
32. L. Platter, H. W. Hammer, and U.-G. Meissner, *Phys. Rev.* **A70**, 052101 (2004), [cond-mat/0404313](#).
33. H. W. Hammer and L. Platter, *Eur. Phys. J.* **A32**, 113 (2007), [nucl-th/0610105](#).
34. J. von Stecher, J. D’Incao, and C. Greene, *Nature Physics* **5**, 417 (2009), [0810.3876](#).
35. F. Ferlaino *et al.*, *Phys. Rev. Lett.* **102**, 140401 (2009).
36. J. von Stecher, (2009), [0909.4056](#).
37. S. Knoop *et al.*, *Nature Physics* **5**, 227 (2009).
38. K. Helfrich and H. W. Hammer, *Europhys. Lett.* **86**, 53003 (2009),

- 0902.3410.
39. M. Zaccanti *et al.*, Nature Physics **5** (2009).
  40. G. Barontini *et al.*, Phys. Rev. Lett. **103**, 043201 (2009), 0901.4584.
  41. N. Gross, Z. Shotan, S. Kokkelmans, and L. Khaykovich, Phys. Rev. Lett. **103**, 163202 (2009).
  42. S. E. Pollack, D. Dries, and R. G. Hulet, (2009), 0911.0893.
  43. M. Bartenstein *et al.*, Phys. Rev. Lett. **94**, 103201 (2005).
  44. T. B. Ottenstein, T. Lompe, M. Kohnen, A. N. Wenz, and S. Jochim, Physical Review Letters **101**, 203202 (2008).
  45. J. H. Huckans, J. R. Williams, E. L. Hazlett, R. W. Stites, and K. M. O'Hara, Phys. Rev. Lett. **102**, 165302 (2009), 0810.3288.
  46. E. Braaten, H. W. Hammer, D. Kang, and L. Platter, Phys. Rev. Lett. **103**, 073202 (2009), 0811.3578.
  47. P. Naidon and M. Ueda, Phys. Rev. Lett. **103**, 073203 (2009).
  48. S. Floerchinger, R. Schmidt, and C. Wetterich, Phys. Rev. A **79**, 053633 (2009).
  49. J. R. Williams *et al.*, Phys. Rev. Lett. **103**, 130404 (2009).
  50. S. R. Beane, P. F. Bedaque, W. C. Haxton, D. R. Phillips, and M. J. Savage, (2000), nucl-th/0008064.
  51. P. F. Bedaque and U. van Kolck, Ann. Rev. Nucl. Part. Sci. **52**, 339 (2002), nucl-th/0203055.
  52. E. Epelbaum, H. W. Hammer, and U.-G. Meissner, Rev. Mod. Phys. **81**, 1773 (2009), 0811.1338.
  53. R. F. Mohr, R. J. Furnstahl, R. J. Perry, K. G. Wilson, and H. W. Hammer, Annals Phys. **321**, 225 (2006), nucl-th/0509076.
  54. E. Braaten and H. W. Hammer, Phys. Rev. Lett. **91**, 102002 (2003), nucl-th/0303038.
  55. E. Epelbaum, Prog. Part. Nucl. Phys. **57**, 654 (2006), nucl-th/0509032.
  56. D. B. Kaplan, M. J. Savage, and M. B. Wise, Nucl. Phys. B **534**, 329 (1998), nucl-th/9802075.
  57. M. C. Birse, J. A. McGovern, and K. G. Richardson, Phys. Lett. **B464**, 169 (1999), hep-ph/9807302.
  58. D. B. Kaplan, Nucl. Phys. **B494**, 471 (1997), nucl-th/9610052.
  59. D. R. Phillips, G. Rupak, and M. J. Savage, Phys. Lett. **B473**, 209 (2000), nucl-th/9908054.
  60. P. F. Bedaque, H. W. Hammer, and U. van Kolck, Nucl. Phys. A **646**, 444



- (1999), nucl-th/9811046.
61. V. F. Kharchenko, Sov. J. Nucl. Phys. **16**, 173 (1973).
  62. H. W. Hammer and T. Mehen, Nucl. Phys. A **690**, 535 (2001), nucl-th/0011024.
  63. I. R. Afnan and D. R. Phillips, Phys. Rev. **C69**, 034010 (2004), nucl-th/0312021.
  64. P. F. Bedaque, G. Rupak, H. W. Griesshammer, and H. W. Hammer, Nucl. Phys. **A714**, 589 (2003), nucl-th/0207034.
  65. H. W. Griesshammer, Nucl. Phys. **A744**, 192 (2004), nucl-th/0404073.
  66. L. Platter and D. R. Phillips, Few Body Syst. **40** (2006).
  67. L. Platter, Phys. Rev. **C74**, 037001 (2006), nucl-th/0606006.
  68. F. Gabbiani, P. F. Bedaque, and H. W. Griesshammer, Nucl. Phys. **A675**, 601 (2000), nucl-th/9911034.
  69. H. W. Griesshammer, Nucl. Phys. **A760**, 110 (2005), nucl-th/0502039.
  70. K. G. Wilson, Rev. Mod. Phys. **55**, 583 (1983).
  71. T. Barford and M. C. Birse, J. Phys. **A38**, 697 (2005), nucl-th/0406008.
  72. M. C. Birse, Phys. Rev. **C77**, 047001 (2008), 0801.2317.
  73. S.-i. Ando and M. C. Birse, Phys. Rev. **C78**, 024004 (2008), 0805.3655.
  74. L. Platter and H. W. Hammer, Nucl. Phys. **A766**, 132 (2006), nucl-th/0509045.
  75. H. Sadeghi and S. Bayegan, Nucl. Phys. **A753**, 291 (2005), nucl-th/0411114.
  76. H. Sadeghi, S. Bayegan, and H. W. Griesshammer, Phys. Lett. **B643**, 263 (2006).
  77. H. Sadeghi, Phys. Rev. **C75**, 044002 (2007), 0704.3793.
  78. H. Sadeghi, (2009), 0908.2052.
  79. H. Sadeghi and S. Bayegan, (2009), 0908.2220.
  80. L. Platter, H. W. Hammer, and U.-G. Meissner, Phys. Lett. **B607**, 254 (2005), nucl-th/0409040.
  81. A. Nogga, H. Kamada, and W. Gloeckle, Phys. Rev. Lett. **85**, 944 (2000), nucl-th/0004023.
  82. E. Epelbaum *et al.*, Phys. Rev. Lett. **86**, 4787 (2001), nucl-th/0007057.
  83. E. Epelbaum *et al.*, Phys. Rev. **C66**, 064001 (2002), nucl-th/0208023.
  84. A. Nogga, S. K. Bogner, and A. Schwenk, Phys. Rev. C **70**, 061002 (2004), nucl-th/0405016.
  85. J. Kirscher, H. W. Griesshammer, D. Shukla, and H. M. Hofmann, (2009), 0903.5538.

86. J. Kirscher, H. W. Griesshammer, D. Shukla, and H. M. Hofmann, (2009), 0909.5606.
87. I. Stetcu, B. R. Barrett, and U. van Kolck, Phys. Lett. **B653**, 358 (2007), nucl-th/0609023.
88. I. Stetcu, B. R. Barrett, U. van Kolck, and J. P. Vary, Phys. Rev. **A76**, 063613 (2007), 0705.4335.
89. I. Stetcu, J. Rotureau, B. R. Barrett, and U. van Kolck, (2009), 0912.3015.
90. S. R. Beane and M. J. Savage, Nucl. Phys. **A717**, 91 (2003), nucl-th/0208021.
91. E. Epelbaum, U.-G. Meissner, and W. Gloeckle, Nucl. Phys. **A714**, 535 (2003), nucl-th/0207089.
92. S. R. Beane, P. F. Bedaque, M. J. Savage, and U. van Kolck, Nucl. Phys. A **700**, 377 (2002), nucl-th/0104030.
93. E. Epelbaum, U. G. Meissner, W. Gloeckle, and C. Elster, Phys. Rev. **C65**, 044001 (2002), nucl-th/0106007.
94. N. Fettes, (2000), Ph.D. Thesis, University of Bonn, Germany, JUL-3814.
95. M. Fukugita, Y. Kuramashi, H. Mino, M. Okawa, and A. Ukawa, Phys. Rev. Lett. **73**, 2176 (1994), hep-lat/9407012.
96. M. Fukugita, Y. Kuramashi, M. Okawa, H. Mino, and A. Ukawa, Phys. Rev. **D52**, 3003 (1995), hep-lat/9501024.
97. S. R. Beane, P. F. Bedaque, K. Orginos, and M. J. Savage, Phys. Rev. Lett. **97**, 012001 (2006), hep-lat/0602010.
98. E. Epelbaum, H. W. Hammer, U.-G. Meissner, and A. Nogga, Eur. Phys. J. **C48**, 169 (2006), hep-ph/0602225.
99. H. W. Hammer, D. R. Phillips, and L. Platter, Eur. Phys. J. **A32**, 335 (2007), 0704.3726.
100. K. G. Wilson, Nucl. Phys. Proc. Suppl. **140**, 3 (2005), hep-lat/0412043.
101. S. R. Beane *et al.*, Phys. Rev. **D80**, 074501 (2009), 0905.0466.
102. S. R. Beane, K. Orginos, and M. J. Savage, Int. J. Mod. Phys. **E17**, 1157 (2008), 0805.4629.
103. S. Kreuzer and H. W. Hammer, Phys. Lett. **B673**, 260 (2009), 0811.0159.
104. S. Kreuzer and H. W. Hammer, (2009), 0910.2191.
105. M. V. Zhukov *et al.*, Phys. Rept. **231**, 151 (1993).
106. C. A. Bertulani, H. W. Hammer, and U. Van Kolck, Nucl. Phys. A **712**, 37 (2002), nucl-th/0205063.
107. P. F. Bedaque, H. W. Hammer, and U. van Kolck, Phys. Lett. **B569**, 159

- (2003), nucl-th/0304007.
108. D. V. Federov, A. S. Jensen, and K. Riisager, Phys. Rev. Lett. **73**, 2817 (1994), nucl-th/9409018.
109. A. E. A. Amorim, T. Frederico, and L. Tomio, Phys. Rev. C **56**, R2378 (1997), nucl-th/9708023.
110. I. Mazumdar, V. Arora, and V. S. Bhasin, Phys. Rev. **C61**, 051303 (2000).
111. D. L. Canham and H. W. Hammer, Eur. Phys. J. **A37**, 367 (2008), 0807.3258.
112. M. T. Yamashita, L. Tomio, and T. Frederico, Nucl. Phys. **A735**, 40 (2004), nucl-th/0401063.
113. F. M. Marques *et al.*, Phys. Rev. **C64**, 061301 (2001), nucl-ex/0101004.
114. D. L. Canham and H. W. Hammer, (2009), 0911.3238.
115. M. T. Yamashita, T. Frederico, and L. Tomio, (2007), 0704.1461.
116. I. Mazumdar, A. R. P. Rau, and V. S. Bhasin, Phys. Rev. Lett. **97**, 062503 (2006), quant-ph/0607193.
117. M. T. Yamashita, T. Frederico, and L. Tomio, Phys. Lett. **B670**, 49 (2008), 0808.3113.
118. A. Cobis, A. S. Jensen, and D. V. Fedorov, J. Phys. **G23**, 401 (1997), nucl-th/9608026.
119. D. V. Fedorov and A. S. Jensen, Nucl. Phys. **A697**, 783 (2002), nucl-th/0107027.
120. J. G. Congleton, J. Phys. **G18**, 339 (1992).
121. H. W. Hammer, Nucl. Phys. **A705**, 173 (2002), nucl-th/0110031.
122. C. A. Bertulani and G. Baur, Phys. Rept. **163**, 299 (1988).
123. V. Efimov, Comm. Nucl. Part. Phys. **19**, 271 (1990).
124. R. Higa, Mod. Phys. Lett. A **24**, 915 (2009), 0809.5157.
125. R. Higa, H. W. Hammer, and U. van Kolck, Nucl. Phys. **A809**, 171 (2008), 0802.3426.
126. H. W. Hammer and R. Higa, Eur. Phys. J. **A37**, 193 (2008), 0804.4643.
127. M. Chernykh, H. Feldmeier, T. Neff, P. von Neumann-Cosel, and A. Richter, Phys. Rev. Lett. **98**, 032501 (2007).
128. E. Eichten, S. Godfrey, H. Mahlke, and J. L. Rosner, Rev. Mod. Phys. **80**, 1161 (2008), hep-ph/0701208.
129. M. B. Voloshin, Prog. Part. Nucl. Phys. **61**, 455 (2008), 0711.4556.
130. S. Godfrey and S. L. Olsen, Ann. Rev. Nucl. Part. Sci. **58**, 51 (2008), 0801.3867.

- 131. Belle, S. K. Choi *et al.*, Phys. Rev. Lett. **91**, 262001 (2003), hep-ex/0309032.
- 132. CDF II, D. E. Acosta *et al.*, Phys. Rev. Lett. **93**, 072001 (2004), hep-ex/0312021.
- 133. D0, V. M. Abazov *et al.*, Phys. Rev. Lett. **93**, 162002 (2004), hep-ex/0405004.
- 134. BABAR, B. Aubert *et al.*, Phys. Rev. **D71**, 071103 (2005), hep-ex/0406022.
- 135. E. Braaten and M. Lu, Phys. Rev. **D76**, 094028 (2007), 0709.2697.
- 136. E. Braaten and M. Lu, Phys. Rev. **D77**, 014029 (2008), 0710.5482.
- 137. E. Braaten, (2008), 0808.2948.
- 138. D. L. Canham, H. W. Hammer, and R. P. Springer, Phys. Rev. **D80**, 014009 (2009), 0906.1263.
- 139. D. V. Bugg, Phys. Lett. **B598**, 8 (2004), hep-ph/0406293.
- 140. C. Hanhart, Y. S. Kalashnikova, A. E. Kudryavtsev, and A. V. Nefediev, Phys. Rev. **D76**, 034007 (2007), 0704.0605.
- 141. M. B. Voloshin, Phys. Rev. **D76**, 014007 (2007), 0704.3029.
- 142. E. Braaten and M. Kusunoki, Phys. Rev. **D69**, 074005 (2004), hep-ph/0311147.